International Journal of Electrochemical Science 19 (2024) 100772

Contents lists available at ScienceDirect

International Journal of Electrochemical Science

journal homepage: www.editorialmanager.com/ijoes

Advanced evaluation of novel quinoline derivatives for corrosion inhibition of mild steel in acidic environments: A comprehensive electrochemical, computational, and surface study

Azzeddine Belkheiri [a], Khadija Dahmani [b], Khaoula Mzioud [a], Mohamed Rbaa [b,c], Mouhsine Galai [a,*], Abdelfettah Hmada [a], Şaban Erdoğan [d], Burak Tüzün [e], Mohamed Ebn Touhami [a], Hamed A. El-Serehy [f], Basheer M. Al-Maswari [g]

[a] Advanced Materials and Process Engineering, Faculty of Sciences, Ibn Tofaïl University, PO Box 133, Kenitra 14000, Morocco
[b] Laboratory of Organic, Inorganic Chemistry, Electrochemistry and Environment, Faculty of Sciences, Ibn Tofaïl University, PO Box 133, Kenitra 14000, Morocco
[c] The Higher Institute of Nursing Professions and Health Techniques of Casablanca, P.O. Box, Casablanca 20250, Morocco
[d] Department of Nutrition and Dietetics, Faculty of Health Sciences, Yalova University, Yalova, Turkiye
[e] Plant and Animal Production Department, Technical Sciences Vocational School of Sivas, Sivas Cumhuriyet University, Sivas, Turkey
[f] Department of Zoology, College of Science, King Saud University, Riyadh 11451, Saudi Arabia
[g] Department of Chemistry, Yuvaraja's College, University of Mysore, Manasagangotri, Mysuru 570006, India

ARTICLE INFO

Keywords:
Mild steel
Hydrochloric acid
Quinoline derivatives
Corrosion inhibitors
Adsorption

ABSTRACT

Corrosion poses a significant threat to the integrity and longevity of iron and its alloys, which are crucial materials for modern industry and infrastructure. This study investigates the effectiveness of two recently synthesized inhibitors based on quinoline structures: MPQ (***2-methyl-5-(propoxymethyl) quinolin-8-ol***) and AAQ ((((***2-aminoethyl)amino)methyl)-2-methylquinolin-8-ol***) in protecting steel against environmental degradation, particularly in acidic and chloride-rich conditions such as hydrochloric acid. The inhibitors exhibited significant corrosion inhibition efficiencies of 92.37 % for MPQ and 84.13 % for AAQ, as demonstrated through electrochemical analysis. Surface characterization techniques, including SEM-EDX(Scanning Electron Microscopy with Energy Dispersive X-ray analysis), AFM (Atomic Force Microscopy), and contact angle measurements, revealed the formation of a protective barrier film that reduces the corrosion rate. Additionally, theoretical calculations using the Gaussian package provided insights into the adsorption behaviors and protective mechanisms of the inhibitors on mild steel surfaces. The findings contribute to the ongoing search for viable corrosion inhibitors, offering prospects for application in industries and critical infrastructures to enhance corrosion protection and durability.

1. Introduction

Iron and its alloys play a crucial role in modern society due to their exceptional physical and chemical properties, such as strong structural integrity and mechanical strength [1,2]. The widespread use of these materials is supported by efficient manufacturing processes and availability. However, corrosion, the gradual deterioration of metal properties when exposed to the environment [3], presents significant challenges [4]. Corrosion is a major global issue, not only threatening critical industries like petrochemicals but also endangering infrastructure such as bridges and public buildings [4,5]. This can lead to catastrophic failures and substantial repair costs [6,7]. The economic impact of corrosion is immense. In 2011, the annual cost of corrosion in the United States alone reached $2.2 trillion, while in India, it exceeded $100 billion. On a global scale, the annual cost of corrosion is estimated at $2.5 trillion, representing approximately 3.4 % of the world's GDP [8].

To address corrosion, methods like acid washing of metal surfaces and acidification of oil wells are commonly employed, often involving the use of corrosive solutions like hydrochloric and sulfuric acids

* Corresponding author.
E-mail addresses: galaimouhsine@gmail.com (M. Galai), saban.erdogan@yalova.edu.tr (Ş. Erdoğan), theburaktuzun@yahoo.com (B. Tüzün), helserehy@ksu.edu.sa (H.A. El-Serehy), basheer.almaswari@gmail.com (B.M. Al-Maswari).

https://doi.org/10.1016/j.ijoes.2024.100772
Received 11 July 2024; Received in revised form 17 August 2024; Accepted 21 August 2024
Available online 25 August 2024

[9–12]. Unfortunately, these acids can accelerate metal erosion, prompting the development of inhibitors as a more advanced and effective protection method [13–16]. Extensive research has focused on identifying effective organic compounds to counter corrosion in highly acidic environments [6,17–19]. Organic corrosion inhibitors typically contain electron-donating atoms like phosphorus, sulfur, oxygen, and nitrogen, which facilitate their adsorption onto metal surfaces, thereby shielding them from acidic solutions [20,21]. These compounds function through various mechanisms, including chemisorption, physisorption, complexation, or precipitation, to block oxygen from reaching the cathode, inhibit hydrogen diffusion from the cathode, or prevent metal dissolution as anodic inhibitors [21,22].

Studies have explored various compounds, including imidazole derivatives, benzimidazole derivatives, quinoline derivatives, as effective corrosion inhibitors [21,23–27]. Quinoline derivatives have emerged as a promising class of corrosion inhibitors, particularly in acidic environments, due to their unique properties and low environmental toxicity. These compounds, which are easy to synthesize and highly water-soluble, have proven extremely effective in protecting metals from corrosion. For instance, El Faydy et al. demonstrated that three 8-hydroxyquinoline derivatives, including 5-propoxymethyl-8-hydroxyquinoline (PMHQ), could reduce carbon steel corrosion by up to 94 %, forming a protective film on the metal surface that limits metal dissolution and hydrogen evolution [28]. Additionally, Jiang et al. confirmed the superior efficacy of the quinoline derivatives BQ and QBPA, with corrosion inhibition reaching 98.03 %, through a mixed adsorption mechanism involving both physisorption and chemisorption, which follows the Langmuir isotherm model [29]. A computational study by Erdoğan et al. revealed that quinoline derivatives can strongly interact with iron surfaces, particularly the Q4 compound, corroborating their experimentally observed inhibitory efficiency [30]. Fakhry et al. studied 5-{[(4-Dimethylamino-benzylidene)-amino]-methyl}-quinolin-8-ol (MABQ) and showed that this mixed-type inhibitor achieves an efficiency of 95.8 % at a concentration of 10^{-3} M by forming a stable protective film on the mild steel surface, consistent with theoretical predictions of adsorption via molecular dynamics simulations [31]. These findings confirm that quinoline derivatives, due to their ability to form robust adsorption barriers on metal surfaces, are prime candidates for the development of new corrosion inhibition solutions.

Furthermore, to enhance the understanding and development of these corrosion inhibitors, computational chemistry tools play a crucial role. Gaussian software package is a key tool used for the calculation of molecular structures and chemical reactions. This program utilizes quantum chemistry methods such as density functional theory (DFT) and molecular orbital theory (MO) [32]. For comparing the activities of molecules, the Gaussian program is used to calculate the energies, structure and interactions of molecular entities [33]. In this context, our study specifically investigates two recently synthesized inhibitors based on quinoline structures for their corrosion inhibition properties in mild steel metal samples immersed in one molar hydrochloric acid. The research delves into the electrochemical mechanisms through which these inhibitors protect the metal samples, supported by multiple characterization techniques such as scanning electron microscopy with energy dispersive X-ray spectroscopy (SEM-EDX), atomic force microscopy (AFM), and contact angle measurements. To compare the activities of corrosion inhibitors, calculations were conducted using the Gaussian package at B3LYP, HF, M062X level with the 6–31++g(d,p) basis set. To determine which corrosion inhibitor is theoretically the most efficient, a molecular dynamics modeling approach was also employed to study the corrosion of iron.

2. Experiment details

2.1. Organic synthesis

The products used in this study were synthesized by reacting 5-(chloromethyl)-2-methylquinolin-8-ol hydrochloride with two nucleophiles. This reaction was carried out in tetrahydrofuran (THF) with triethylamine (Et_3N) as a base and was allowed to proceed for 12 hours (Fig. 1). The synthesized products were subsequently characterized using nuclear magnetic resonance spectroscopy.

2.2. Materials and sample preparation

To prepare a solution with significant properties, such as a 1.0 M HCl solution, an analytical reagent-grade 37 % HCl solution was diluted with double-distilled water. The experimental setup involved using the two synthesized inhibitors, MPQ and AAQ (Fig. 1), at concentrations ranging from 10^{-3} M to 10^{-6} M. Additionally, a blank solution was carefully prepared for comparison purposes. The metal samples, whose composition is detailed in Table 1, were meticulously prepared by abrasion with emery paper of various particle sizes, followed by washing with distilled water, degreasing with ethanol and air-drying at room temperature. The surface area exposed to the corrosive medium during the tests was 1 cm^2.

2.3. Electrochemical investigations

Electrochemical measurements, including potentiodynamic polarization (PDP) and electrochemical impedance spectroscopy (EIS), are employed to study material corrosion. The potentiostat controls the electrode potential relative to a reference electrode, while the galvanostat regulates the current. The PGZ 100 is a notable potentiostat/galvanostat instrument used in these experiments. For the experiment, a platinum sheet serves as the counter electrode and an Ag/AgCl electrode is used as the reference. The working electrode represents the samples, and precise positioning is crucial for reproducibility. The open circuit potential (OCP) is established by immersing the working electrode in the test solution without applying an external potential, providing information on system stability and susceptibility to corrosion. Potentiodynamic polarization experiments on mild steel specimens involved automated adjustment of electrode potential, ranging from −0.9 to −0.1 V/Ag/AgCl versus OCP, at a scan rate of 1 mV/s. Corrosion current density was determined by extrapolating the Tafel linear segments from anodic and cathodic curves. This corrosion current density was then correlated with the corrosion potential (E_{corr}). The assessment of inhibitory effectiveness was performed using the following equation (Eq. 1) [19,34]:

$$\eta_{PDP}\% = \left[1 - \frac{i_{corr}}{i^{\circ}_{corr}}\right] \times 100 \quad (1)$$

Where i_{corr} stands for the corrosion current density observed in the presence of an inhibitor, and i°_{corr} represents the corrosion current density observed in the absence of the inhibitor. A higher inhibition efficiency indicates a more effective inhibitor in terms of corrosion prevention.

Electrochemical Impedance Spectroscopy (EIS) measurements were performed using a transfer function analyzer and a low-amplitude alternating current signal (10 mV/ms). The frequency range spanned from 100 kHz to 100 mHz, with 10 data points per logarithmic decade. An analysis of the acquired data was executed using EC-Lab software, which employs an analogous electrical circuit model for interpretation. The following equation (Eq. 2) was used to evaluate the inhibitory effectiveness in this case [19,34]:

$$\eta_{imp} = \left[1 - \frac{R^{\circ}_{CT}}{R_{CT}}\right] \times 100 \quad (2)$$

Where R_{CT} and R°_{CT} represent the relative charge transfer resistances in the presence of the inhibitor and R°_{CT} represent the relative charge transfer resistances in the absence of the inhibitor. Comparing these

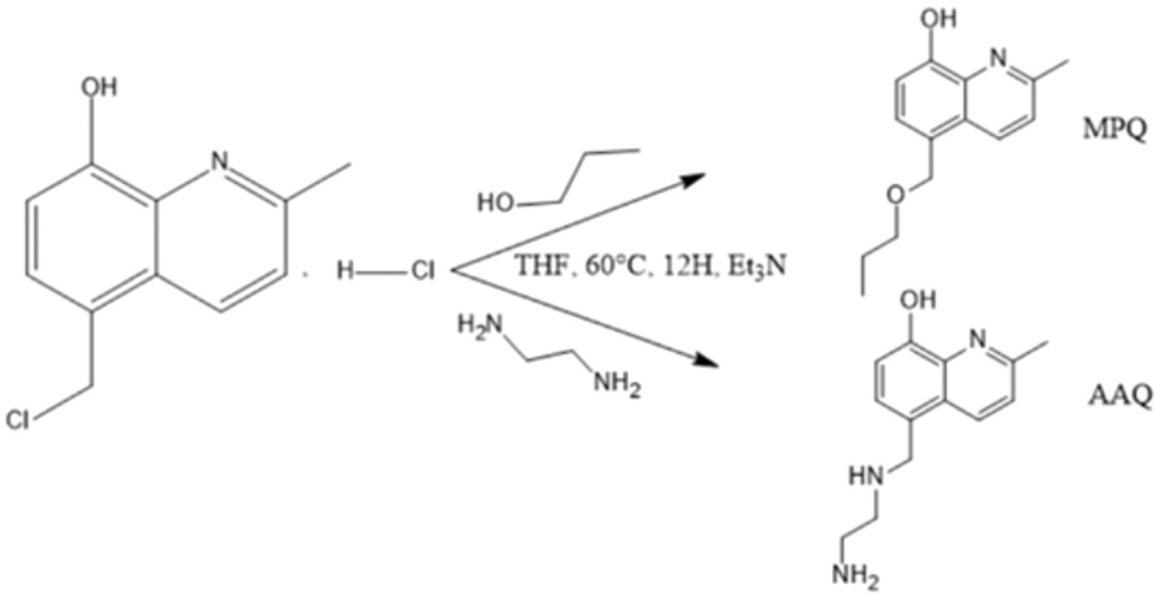

Fig. 1. Method for preparing organic inhibitors synthesis.

Table 1
The weight percentages of elemental composition in mild steel.

Material	Chemical composition											
	C	Si	Mn	Cr	Mo	Ni	Al	Cu	Co	V	W	Fe
Metal	0,11	0,24	0,47	0,12	0,02	0,1	0,03	0,14	<0,0012	<0003	0,06	Balance

resistances provides insights into how the inhibitor affects the charge transfer processes occurring at the electrode-electrolyte interface. A higher value of R_{CT} indicates a greater resistance to charge transfer, which signifies better inhibition efficiency [34]. This approach enables us to understand the complex electrochemical behavior influenced by the presence of the inhibitor.

2.4. Morphological study (MEB-EDX/AFM)

To study in detail the surface properties, steel coupons of precise dimensions (1.0 cm × 1.0 cm × 0.1 cm) were manufactured. These coupons were immersed in a solution containing 1.0 M HCl, as well as specific concentrations of MPQ and AAQ (10^{-3} M) and maintained in this solution for 24 hours. The objective was to understand the impact of these chemical substances on the surface characteristics of the steel. The prepared samples were then subjected to analysis by Scanning Electron Microscopy (Quattro ESEM) and EDX analysis to obtain high-resolution images of the surface structure and elemental composition of the samples. In addition, to examine the morphology of the deposited films, a Veeco Dimension ICON atomic force microscope, manufactured by Bruker, was employed. The surface features of these films were investigated under typical pressure and temperature conditions. AFM images were acquired in accordance with these settings. All these experiments were conducted at the MAScIR-Rabat research center, a leading institution in the field of research.

2.5. Contact angle

To study the wettability, we used the OCA 40 Micro, accompanied by the ES Nano-drop electronic dosing device and the Up HSC 2000 high-speed camera system. After depositing the liquid on the coated surface for one minute, we measured the water contact angles (WCA) based on the drop profile once equilibrium was reached.

2.6. Theoretical methods

Theoretical calculations provide important information about the chemical properties of molecules. Many quantum chemical parameters are obtained from theoretical calculations. The calculated parameters are used to explain the chemical activities of the molecules. Many programs are used to calculate molecules. These programs are Gaussian09 RevD.01 and GaussView 6.0 [35,36]. By using these programs, calculations were made in B3LYP, HF, and M06–2x [37–39]. Methods with the 6–31++g(d,p) basis set. As a result of these calculations, many quantum chemical parameters have been found. Each parameter describes a different chemical property of molecules, the calculated parameters are calculated as follows [40,41].

$$\chi = -\left(\frac{\partial \mathrm{E}}{\partial N}\right)_{\upsilon(r)} = \frac{1}{2}(I+A) \cong \frac{1}{2}\left(E_{HOMO}+E_{LUMO}\right) \quad (3)$$

$$\eta = -\left(\frac{\partial^2 \mathrm{E}}{\partial N^2}\right)_{\upsilon(r)} = \frac{1}{2}(I-A) \cong -\frac{1}{2}(E_{HOMO}-E_{LUMO}) \quad (4)$$

$$\sigma = 1/\eta\omega = \chi^2/2\eta\varepsilon = 1/\omega$$

2.7. Molecular dynamic (MD) Simulation

Monte Carlo (MC) simulation was employed to investigate the interaction of 5a and 5d with the mild steel surface [42]. Consequently, the adsorption locator module of the Materials Studio software was utilized to examine how these molecules interacted with the Fe (110) surface [43]. All adsorption calculations of the systems were performed using the COMPASS force field due to its effectiveness in the field of corrosion modeling. Initially, a crystal of Fe (110) was created, and then the optimized structure of 5a and 5d was examined to obtain the most stable adsorbed configurations on the Fe (110) surface in the presence of water molecules [44,45].

3. Results and Discussion

3.1. Chemical study

The chemical shift values (δ_{ppm}) of the proton and carbon atoms obtained from the proton and carbon NMR spectra (^{1}H NMR and ^{13}C NMR) are illustrated below:

2-methyl-5-(propoxymethyl) quinolin-8-ol (MPQ)

^{1}H NMR (JNM-ECZ500R/S1 FT NMR System de JEO, DMSO-d_6) (δ_{ppm}): 3.709 (s, 1 H, OH), 5.718–7.777 (m, 5 H, ArH), 3.304–3.703 (m, 6 H, CH_2), 4.471 (s, 3 H, CH_3). ^{13}C NMR (JNM-ECZ500R/S1 FT NMR System de JEO, DMSO-d_6) (δ_{ppm}): 82.046 (C-OH), 105.103–111.270 (ArCH, ArC), 14.472–31.811(C-CH_2).

5-(((2-aminoethyl)amino)methyl)-2-methylquinolin-8-ol (AAQ)

^{1}H NMR (JNM-ECZ500R/S1 FT NMR System de JEO, DMSO-d_6) (δ_{ppm}): 3.310 (s, 1 H, OH), 5.717–5.775 (m, 5 H, ArH), 3.421–4.467 (m, 6 H, CH_2), 4.475 (s, 3 H, CH_3). ^{13}C NMR (JNM-ECZ500R/S1 FT NMR System de JEO, DMSO-d_6) (δ_{ppm}): 82.058 (C-OH), 104.986–111.265 (ArCH, ArC), 14.460–31.815(C-CH_2), 80.892 (C-NH_2).

3.2. Electrochemistry tests

3.2.1. Potentiodynamic Polarization Test

To gain insights into the kinetics of cathodic and anodic processes, a series of polarization studies were conducted in unstirred solutions containing 1.0 M HCl. These experiments were performed both in the absence of organic products (MPQ and AAQ) and with with varying concentrations of these compounds. The polarization curves obtained are shown in Fig. 2.

The electrochemical parameters provided in Table 2, especially the corrosion potential (E_{corr}), cathodic and anodic Tafel slopes (βc, β_a), and corrosion current density (i_{corr}), were calculated using the extrapolation of the anodic and cathodic Tafel curves.

Table 2
Corrosion values determined by PDP of mild steel in 1.0 M HCl without and with MQP and AAQ at 298 K.

Medium	Conc. (M)	- E_{corr} mV/Ag /AgCl	i_{corr} µA cm^{-2}	-β_c mV dec^{-1}	β_a mVdec^{-1}	Θ	η_{pp} %
1.0 M HCl	–	498	983	140	150	–	–
MPQ	10–6	487	198	179	113	0.7985	79.85
	10–5	494	124	173	108	0.8738	87.38
	10–4	486	82	163	101	0.9165	91.65
	10–3	480	75	168	88	0.9237	92.37
AAQ	10–6	497	242	174	118	0.7538	75.38
	10–5	480	202	165	109	0.7945	79.54
	10–4	494	169	159	106	0.8280	82.80
	10–3	491	156	157	97	0.8413	84.13

Upon thorough examination of Fig. 2 and Table 2, it was noted that untreated mild steel exhibited the highest anodic and cathodic current densities. However, the introduction of the quinoline derivatives MPQ and AAQ led to a marked decrease in these current densities. This suggests that the inhibitors significantly reduce the corrosion rate of steel in a 1 M HCl environment by lowering the anodic dissolution of mild steel and delaying the reduction of H+ ions [6,46,47]. As the concentration of the inhibitors increased, the cathodic branches in the polarization curves appear nearly parallel (Fig. 2), indicating that MPQ and AAQ do not alter the fundamental mechanism of the cathodic reaction, they effectively slow down its kinetics, particularly the hydrogen evolution process [4,6,34,48]. The similarity in cathodic slope values (βc) (Table 2) suggests that the hydrogen evolution reaction is primarily controlled by an activation mechanism at the metal/solution interface, involving charge transfer [49–51]. Moreover, the minimal impact of the inhibitors on the anodic reaction when the potential exceeds the desorption potential (-300 mV) aligns with findings by Al-Moubaraki et al.[52].This phenomenon can be attributed to the increased surface area exposed as the steel corrodes, leading to the desorption of the inhibitor molecules[52,53]. At potential exceeding −300 mV, the inhibitors facilitate significant metal surface dissolution, resulting in a desorption rate of adsorbed molecules that exceeds their adsorption rate. Additionally, a slight anodic shift in the corrosion potential was observed with the inhibitors, indicating that their presence in the acidic solution impacts both the hydrogen evolution and metal dissolution processes [53]. The anodic slope values (βa) exhibit minimal changes in the presence of MPQ and AAQ, which indicates that these inhibitors limit corrosion by reducing the number of active sites on the mild steel surface without fundamentally altering the anodic or cathodic processes [54–56]. Consequently, the presence of these inhibitors in the corrosive

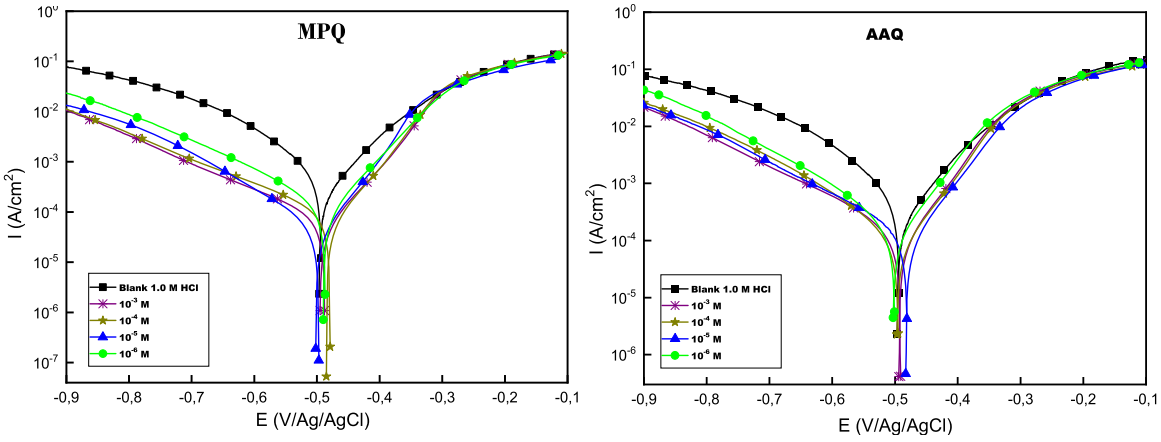

Fig. 2. The polarization curves of mild steel immersed in an aggressive solution, both in the absence and in presence of different concentrations of MPQ and AAQ, at a temperature of 298 K.

solution significantly slows hydrogen evolution at the cathode and metal dissolution at the anode [57–59]. The minor shift in corrosion potential (-18 mV for MPQ and −7 mV for AAQ, both well below 85 mV) classifies these inhibitors as pickling-type [46,55,60].

The data presented in Table 2 reveal a clear pattern: the presence of MPQ and AAQ reduces i_{corr} values while enhancing their respective inhibition efficiencies (η_{pp} %). Specifically, the η_{pp} % reaches 92.37 % for MPQ and 84.13 % for AAQ, both at a concentration of 10^{-3} M. These findings highlight that MPQ is a more effective inhibitor than AAQ. This difference in effectiveness can be attributed to the distinct chemical structures of the two molecules: the bulky and hydrophobic propoxymethyl group in MPQ facilitates better adsorption and forms a more compact protective layer on the metal surface. Conversely, the more hydrophilic aminoethyl group in AAQ, despite its ability to form hydrogen bonds, makes the molecule less capable of creating a continuous hydrophobic barrier, thereby reducing its corrosion protection effectiveness compared to MPQ. Nonetheless, both inhibitors adsorb onto the surface, forming a barrier that restricts the movement of ions and electrons [16].

3.2.2. Electrochemical Impedance Spectroscopy Test

The Nyquist plots (Fig. 3) exhibit a depressed semi-circular pattern, which can be attributed to surface modifications. Furthermore, the capacitive nature of the corrosion reactions is indicated by the presence of a semicircular arc. As the concentrations of MPQ and AAQ increase, the length of the semicircular arc also increases, signifying a rise in the steel's charge transfer resistance (R_{ct}) [61–64]. The double layer capacitance (C_{dl}) was calculated using Eq. 5 [34,65]:

$$C_{dl} = \sqrt[n]{A(R_{ct})^{1-n}} \quad (5)$$

The schematic representation of the electrical equivalent circuit utilized in the analysis is depicted in Fig. 4.

The EIS values calculated are shown in Table 3. According to Table 3, increasing the concentrations of MPQ and AAQ results in an increase in R_{ct} and a decrease in C_{dl}, respectively. This observation is consistent with the adsorption of AAQ and MPQ, which displaces the previously adsorbed water molecules [6,64,66]. At the optimal concentration (10^{-3} mol/L), the maximum R_{ct} values are 432.8 Ω cm^2 for MPQ and 200.3 Ω cm^2 for AAQ. It's worth highlighting that MPQ exhibits superior inhibitory properties compared to AAQ. The calculated inhibition efficiencies at the maximum concentration for MPQ and AAQ are 91.98 % and 82.67 % respectively.

3.2.3. Bode

Fig. 5 display Bode diagrams comparing samples with and without AAQ and MPQ. Analysis of these diagrams indicates a notable upward

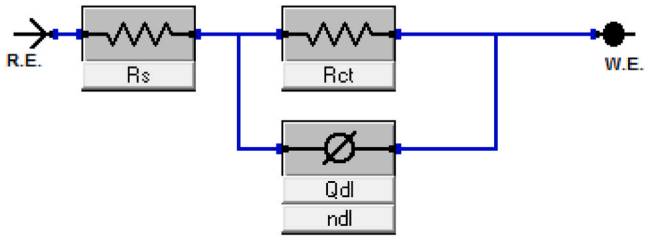

Fig. 4. Equivalent circuits compatible with experimental impedance data.

trend in phase angle values within the intermediate frequency range when AAQ and MPQ are present, as opposed to the blank sample. This trend suggests the development of a protective corrosion inhibitor layer, thereby enhancing the capacitive properties of the mild steel [67,68]. Moreover, the phase angle values observed being less than 90°, indicate deviations from ideal capacitive behavior, thereby affirming the presence of inhomogeneities within the system [69]. Likewise, the Bode plots suggest that at lower frequencies, impedance values increase proportionally with the concentration of AAQ and MPQ. This corresponds to the adsorption of inhibitors onto the steel surface, effectively preventing corrosion [54,70,71].

As noted, the phase angle does not reach 90°, indicating that the system is not purely capacitive. The observed angle below 90° can be attributed to the complex impedance behavior, which includes contributions from both capacitive and resistive elements [72,73]. This behavior is consistent with the mixed adsorption mechanism of AAQ and MPQ, where the inhibitors partially block the steel surface, reducing corrosion but not entirely eliminating the resistive component of the impedance.

Moreover, the Rmin value in the impedance spectra corresponds to the charge transfer resistance (Rct), a key parameter in evaluating the effectiveness of the corrosion inhibitors. The increase in Rmin with increasing inhibitor concentration reflects the improved protection offered by the inhibitors, as they reduce the rate of electron transfer between the steel and the corrosive environment [69,74].

3.2.4. Effect of temperature on inhibition

The temperature of the environment in which a material is exposed to corrosion significantly influences its behavior [75,76]. It's commonly noted that as temperature increases, the inhibitory effect tends to decrease [46,77]. This widely observed phenomenon is fundamental to corrosion studies. Additionally, understanding how temperature affects inhibitor absorption provides crucial insights into their mechanism of action [15,34,78]. In the specific case of the Potentiodynamic Polarization Potential (PDP) experiment, conducted across a temperature range of 298–328 kelvins, a thorough investigation was conducted to

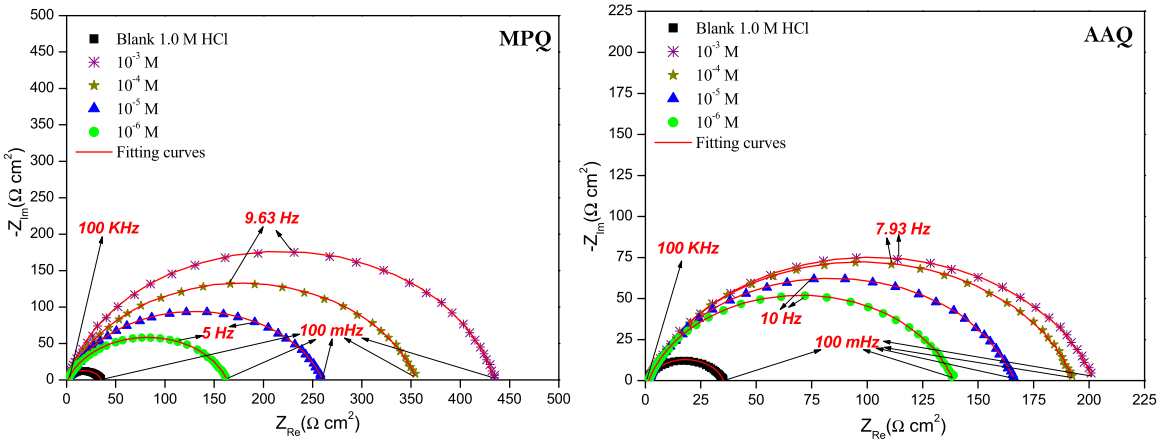

Fig. 3. Effect of MPQ and AAQ Concentrations on Nyquist Plots of Mild Steel in 1.0 M HCl Solution.

Table 3
Electrochemical parameter values for Mild Steel in 1.0 M HCl solution with varying concentrations of MPQ and AAQ.

Medium	Conc. (M)	R_s (Ω cm^2)	R_{ct} (Ω cm^2)	C_{dl} (μF.cm^{-2})	n_{dl}	Q (μF.Sn-1)	Θ	η_{imp} %
1.0 M HCl	–	1.12	34.7	121	0.773	419	–	–
MPQ	10^{-6}	1.37	161.7	82	0.822	189	0.7854	78.54
	10^{-5}	1.36	258.8	58	0.813	99	0.8659	86.59
	10–4	1.32	354.2	32	0.811	79	0.9020	90.20
	10–3	1.70	432.8	25	0.817	45	0.9198	91.98
AAQ	10–6	1.60	137.1	93	0.832	143	0.7469	74.69
	10–5	1.58	164.8	84	0.829	125	0.7894	78.94
	10–4	1.57	191.3	65	0.818	118	0.8186	81.86
	10–3	1.69	200.3	60	0.823	114	0.8267	82.67

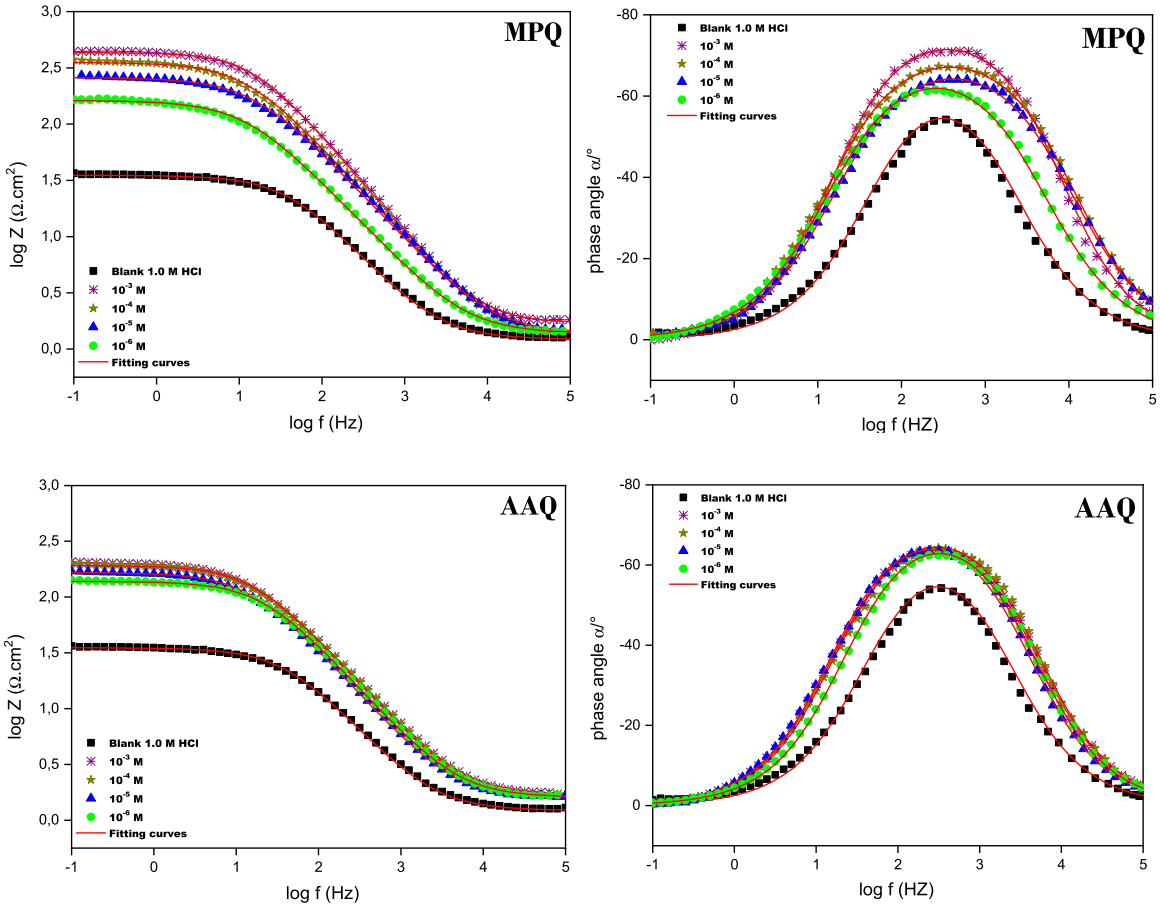

Fig. 5. Bode Plots for Mild Steel with and without varying MPQ and AAQ concentrations in 1.0 M HCl Solution.

elucidate the detailed impact of temperature on inhibition efficiency (IE %).

As a result, we observe that with an increase in temperature, the corrosion current (i_{corr}) rises, as shown in both Fig. 6 and Table 4. This increase is more pronounced in the uncontrolled solution. Furthermore, we noted a slight decrease in the inhibitory effectiveness of the studied compounds with the rise in temperature. This suggests that the temperature increase did not significantly affect the adsorption of MPQ and AAQ onto the steel surface [6,16,17,48]. As temperature increases, the balance between adsorption and desorption tends to shift toward desorption [79,80]. Consequently, there is a marginal decrease in the efficiency of MPQ and AAQ molecules. This shift occurs as the equilibrium moves away from adsorption and toward desorption during the process [17,80].

3.2.5. *Electrochemical Frequency Modulation*

Electrochemical Frequency Modulation (EFM) is a non-intrusive method for measuring corrosion, offering insights into corrosion current without the prerequisite knowledge of the Tafel constant [81]. EFM operates by employing small alternating signals, akin to Electrochemical Impedance Spectroscopy (EIS). However, unlike EIS, EFM simultaneously applies two distinct sinusoidal waves to the cell, resulting in a nonlinear system response due to the nonlinear relationship between current and potential [82]. Apart from the two input frequencies, the current response includes frequency components such as the sum, difference, and multiples of the two input frequencies [83]. The selection of these frequencies likely wasn't arbitrary, given their very slight integer multiples of a base frequency. Intermodulation spectra, as depicted in Fig. 7, were extrapolated from EFM experiments in the presence and the absence of MPQ and AAQ. The kinetic parameters of corrosion, outlined in Table 5, were derived employing the EFM approach and pertinent

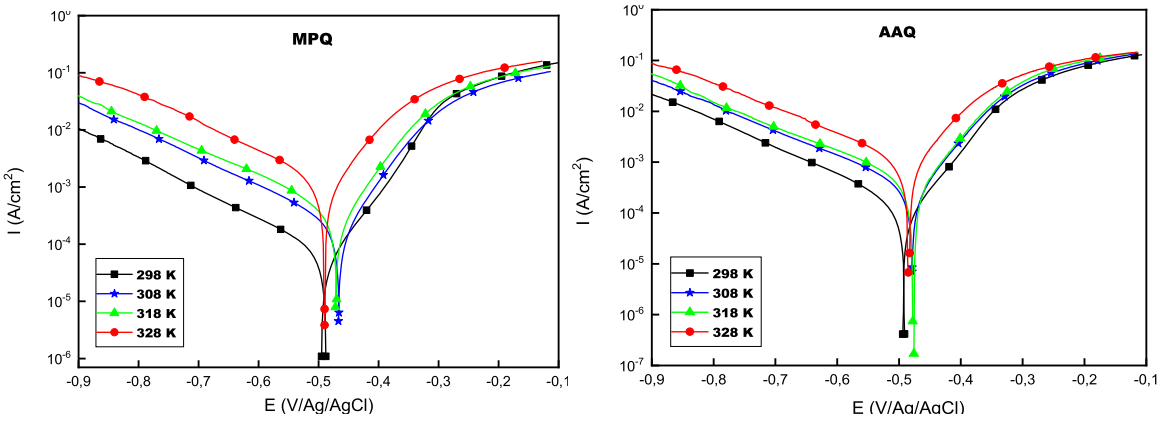

Fig. 6. Potentiodynamic polarization plots for MS in 1.0 M HCl with 10^{-3} M of MPQ and AAQ at various temperatures.

Table 4
Electrochemical and associated factors influencing the inhibitory efficiency of mild steel studied at the optimum concentration of MPQ and AAQ in the temperature range.

Medium	Temperature K	-E_{corr} (mV/Ag /AgCl)	i_{corr} (μA cm-2)	-β_c (mV dec-1)	β_a (mV dec-1)	ηpp
Blank	298	498	983	140	150	-
	308	491	1200	184	112	-
	318	475	1450	171	124	-
	328	465	2200	161	118	-
MPQ	298	480	75	168	88	92.37
	308	465	122	151	107	89.83
	318	469	173	161	117	88.06
	328	491	331	162	125	84.95
AAQ	298	491	156	157	97	84.13
	308	478	213	146	105	82.25
	318	479	271	149	111	81.31
	328	485	442	163	129	79.90

equations:

$$i_{corr} = \frac{i_{\omega}^2}{\sqrt{48(2i_{\omega}i_{3\omega} - i_{2\omega})}} \quad (6)$$

$$\beta_a = \frac{i_{\omega}U_0}{2i_{2\omega} + 2\sqrt{3}\sqrt{2i_{\omega}i_{\omega} - i_{2\omega}^2}} \quad (7)$$

$$\beta_a = \frac{i_{\omega}U_0}{2\sqrt{3}\sqrt{2i_{3\omega}i_{\omega} - i_{2\omega}^2 - 2i_{2\omega}}} \quad (8)$$

$$Casuality\ factor(2) = \frac{i_{\omega_2} \pm \omega_1}{i_{2\omega_1}} = 2.0 \quad (9)$$

$$Casuality\ factor(3) = \frac{i_{2\omega_2} \pm \omega_1}{i_{3\omega_1}} = 3.0 \quad (10)$$

$$E_{EFM}\ \% = 1\frac{-i_{corr}}{i_{corr}^0} \times 100 \quad (11)$$

Here, i_{ω} stands for the current density at the working electrode, MS, recorded at frequency ω, and U_0 represents the amplitude of the sine wave distortion.

According to Table 5, the reduction in i_{corr} values can be attributed to the adsorption of MPQ and AAQ molecules [84]. The inhibition efficiency via this method follows the order: AAQ<MPQ. The causality factors (CF-2 and CF-3) presented in Table 5 closely align with theoretical values of 2.0 and 3.0, respectively, affirming the reliability of the obtained results [34,85]. Also, we observe minimal changes in the values of β_a and β_c, suggesting that the mechanism of both anodic and cathodic reactions remains unaffected by the addition of our inhibitors [19,34].

3.3. Adsorption mechanism for corrosion inhibition

The adsorption mechanisms of MPQ and AAQ on steel immersed in a 1.0 M HCl solution were investigated. Our aim was to assess the degree and nature of interaction between the inhibitors and steel surface morphology, using adsorption isotherms. This investigation involved analyzing obtained data using diverse adsorption models, namely Langmuir, Freundlich, Temkin, and Frumkin [86–88]. The correlation between the recovery rate and the concentrations of MPQ and AAQ is outlined in Table 6, where 'f' represents the energy inhomogeneity factor, with a positive value indicating lateral attraction between the adsorbed species, while a negative value implies repulsion [34,47]. The equilibrium constant for adsorption processes is denoted by K_{ads}, with C_{inh} representing the concentration of the products under examination [47,89]. The parameter 'n' signifies the adsorption intensity, while 'θ' corresponds to the rate of coverage of the steel surface by the adsorbed inhibitor. The 'θ' values were obtained from the impedance results, and the fitting of various isotherms is presented in Fig. 8.

The findings, showcased in both Fig. 8 and Table 6, demonstrate a robust conformity with the Langmuir adsorption isotherm. The model exhibits an outstanding alignment with experimental data, characterized by slopes and correlation coefficients approaching unity, thus indicating its aptness in delineating the adsorption characteristics of our inhibitors [15,78]. As per this model, MPQ and AAQ are capable of adsorbing onto the steel surface, forming a protective barrier film that aids in shielding the steel from corrosion [90]. For the Temkin, Frumkin, and Freundlich models, which assume non-ideal adsorption processes, the correlation coefficients also closely approach unity. Both the ''f'' parameter of the Frumkin isotherm and the ''f'' parameter of the Temkin isotherm are negative, indicating lateral attraction among the adsorbed species [47]. Additionally, the value of 'n' obtained for the Freundlich model significantly deviates from the standard reference value of 0.6, indicating that the studied adsorption mechanism cannot be adequately described by the Freundlich isotherm, despite an R^2 value meeting standard criterion [34]. The adsorption equilibrium constant (K_{ads}) is linked to the standard free adsorption energy (ΔG_{ads}) through formula (Eq. 12) [90–92].

$$\Delta G_{ads} = -RT\ln(55.5K_{ads}) \quad (12)$$

In the given context, 'R' symbolizes the universal gas constant, 'T' denotes the temperature, and '$C_{solvent}$' represents the concentration of the solvent, particularly water, in the solution, which remains constant at 55.5 mol per liter. As commonly understood, an electrostatic

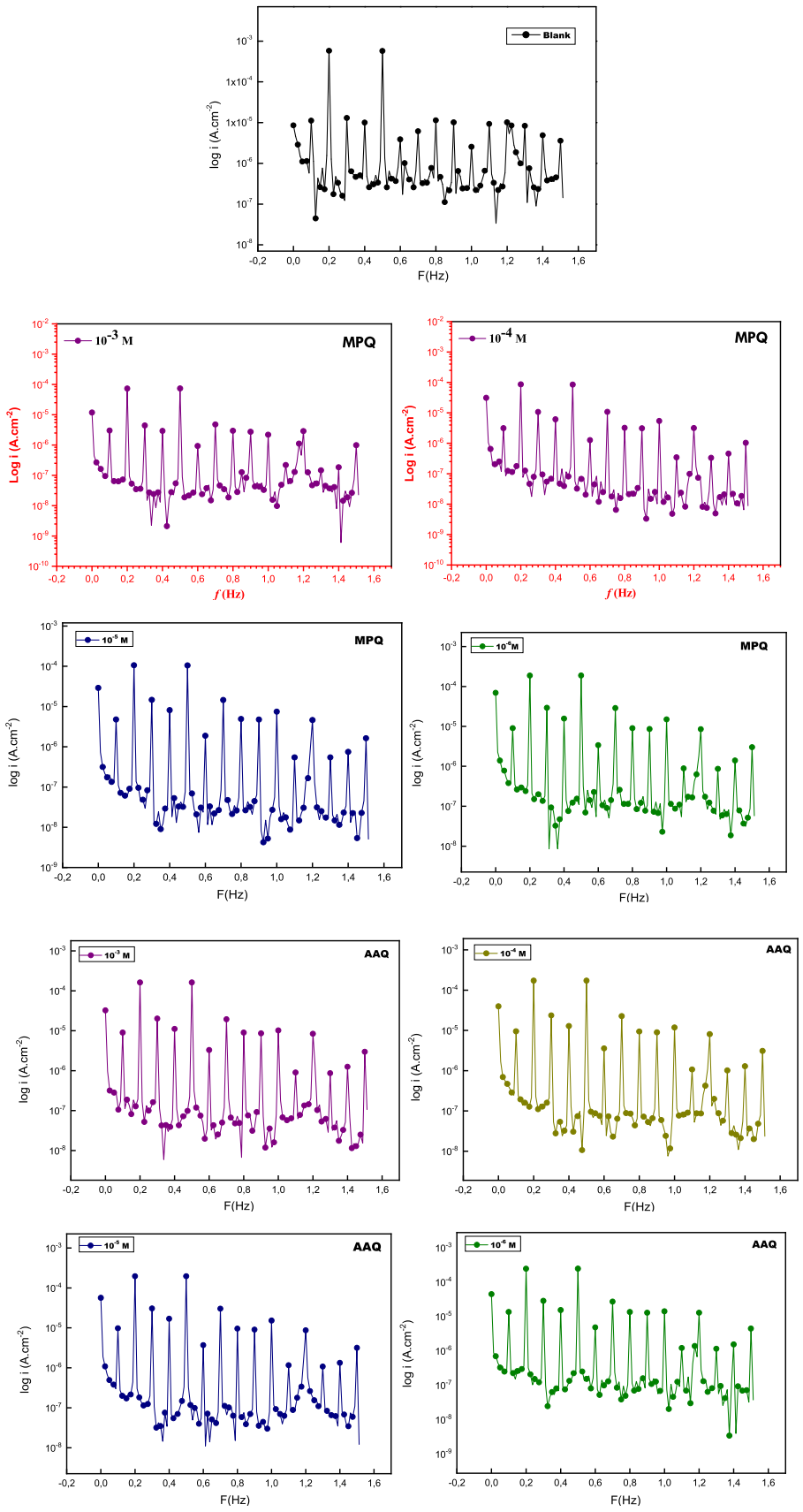

Fig. 7. Electrochemical frequency modulation trend curves in the presence and absence of all the studied concentration of MPQ and AAQ.

Table 5
EFM Analysis of Mild Steel with and without MPQ and AAQ at 298 K.

Medium	Conc. (M)	i_{corr} μAcm-2	-βc mVdec-1	βa mVdec-1	CR, mm y-1	η %	CF-2	CF-3
1.0 M HCl	-	755	177	162	344.9	-	-	-
MPQ	10^{-6}	170.7	164	106	77.99	77.39	1.88	2.74
	10^{-5}	96.64	157	104	43.62	87.22	1.87	2.71
	10^{-4}	85.75	174	94	39.18	88.64	1.86	2.75
	10^{-3}	66.67	133	92	30.46	91.16	1.80	3.02
AAQ	10^{-6}	195.2	127	88	89.18	74.14	1.88	2.84
	10^{-5}	177.2	163	91	80.99	76.52	1.89	2.70
	10^{-4}	142.9	139	85	65.30	81.07	1.87	2.69
	10^{-3}	130.8	130	87	59.87	82.67	1.85	2.79

Table 6
Adsorption parameters from studied isotherms of MPQ and AAQ.

Isotherms	*Equation*	*linear form*	*Parameters*	*MPQ*	*AAQ*
Langmuir	$k_{ads}c_{inh} = \frac{\theta}{1-\theta}$	$\frac{C_{inh}}{\theta} vs C_{inh}$	R^2	1	1
			Slope	1.086	1.209
			K (L/mol)	1.0050 E+06	1.5790 E+06
			ΔG_ads (kJ/mol)	−44.19	−45.31
Freundluich	$\theta = k_{ads}C_{inh}^{n}$	$\ln(\theta) vs \ln(C_{inh})$	R^2	0.8931	0.9178
			Slope (n)	0.02235	0.0148
			K (L/mol)	1.093	0.9265
			ΔG_ads (kJ/mol)	−10.2	−9.76
Temkin	$e^{-2f\theta} = k_{ads}C_{inh}$	$\theta vs \ln C_{inh}$	R^2	0.9046673	0.92348256
			Slopes (−1/2 f)	0.01908	0.01167
			f	−26.2055	−42.8449
			K (L/mol)	1.83 E+24	1.26 E+34
			ΔG_ads (kJ/mol)	−148.4	−204.5
Frumkin	$\frac{\theta}{1-\theta}e^{-2f\theta} = k_{ads}C_{inh}$	$\ln\left(C_{inh}\frac{1-\theta}{\theta}\right) vs \theta$	R^2	0.87960014	0.91282738
			Slopes (2 f)	−39.11	−73.16
			f	−19.5552	−36.5812
			K (L/mol)	1.25 E+20	2.33 E+30
			ΔG_ads (kJ/mol)	−124.6	−183.2

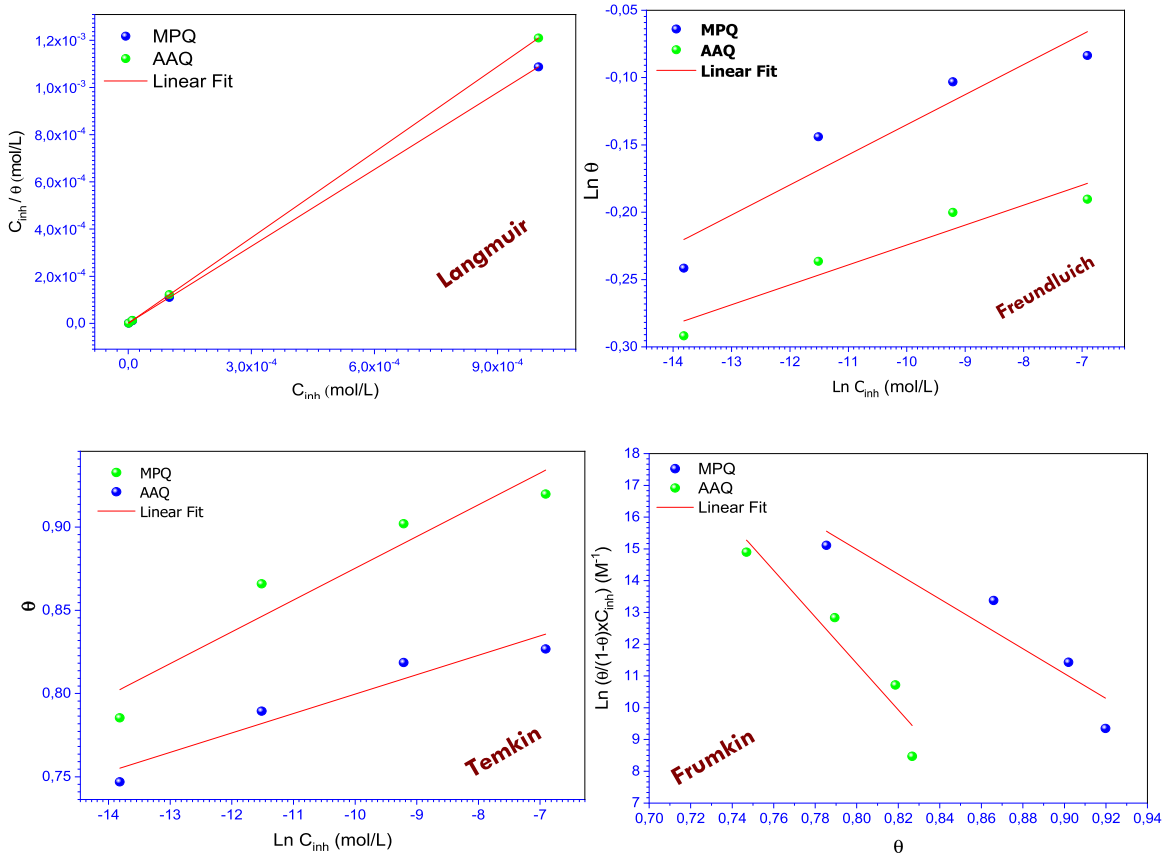

Fig. 8. Adsorption Isotherms of Mild Steel in 1.0 M HCl with MPQ and AAQ.

interaction typically arises between the organic species and the charged metal, known as physisorption, when the obtained values approach −20 kJ mol^{-1} [15,78]. Conversely, a charge transfer from the organic species to the metal surface, termed chemisorption, occurs when the ΔG_{ads} values are approximately −40 kJ mol^{-1} [15,78]. In this study, the computed values from the ΔG_{ads} for the Langmuir model are around −40 kJ mol^{-1} for both organic species, indicating that both inhibitors undergo chemisorption onto the surface of the mild steel. This results in the formation of bonds that effectively resist the penetration of corrosive chloride species.

3.4. Corrosion kinetic parameters

According to the Arrhenius equation and the transition state formula, it is possible to determine the activation energy of the corrosion process (E_a) and the values of ΔH_a and ΔS_a at different temperatures in the absence and presence of MPQ and AAQ. This can be achieved by studying the impact of temperature on corrosion current density (i_{corr}) [4,16]:

$$i_{corr} = Ae^{\frac{-Ea}{RT}} \quad (13)$$

$$\ln\left(\frac{i_{corr}}{T}\right) = \left[\ln\left(\frac{R}{hN_a}\right) + \left(\frac{\Delta S_a}{R}\right)\right] - \frac{\Delta H_a}{RT} \quad (14)$$

Where E_a represents the activation energy (kJ.mol^{-1}), i_{corr} represents the corrosion current density in mA.cm^{-2}, R represents the ideal gas constant (8.314 J.mol^{-1}.K^{-1}), A is the Arrhenius pre-exponential constant, T is the absolute temperature in Kelvin (K) and Na represents Avogadro's number and h Planck's constant. In addition, ΔH_a represents the enthalpy of activation and ΔS_a the entropy of activation.

Figs. 9a and 9b show the variation of E_a and ΔH_a in the absence and presence of MPQ and AAQ at 10^{-3} M, respectively, with roughly parallel lines. Table 7 shows a compilation of the activation parameters obtained from Figs. 9a and 9b.

Table 7 illustrates that activation energy (E_a) values in solutions containing the compounds under investigation, demonstrate elevated values compared to those observed in the uninhibited solution. This increase in activation energy (E_a) when an inhibitor is present can be attributed to a heightened energy barrier [19,34]. This observation further confirms the formation of a complex compound between the inhibitor and the mild steel, indicating the development of an adsorptive film in contrast to the uninhibited solution [14,47]. Additionally, the rise in activation energy E_a compared to the blank suggests a preference for electrostatic interactions with the metal surface, with the adsorption of the protective film being primarily physical in nature [16,93]. As a result, the inhibitors examined adhere to the steel surface, creating a protective film that acts as a barrier, limiting the penetration of corrosive agents onto the metal surface. The slowness of the steel dissolution process in the presence of MPQ and AAQ is underscored by the positive ΔH_a values, indicating the endothermic nature of the degradation process [47,94].

Table 7
Thermodynamic parameters of inhibition study in the presence and absence of MPQ and AAQ.

Medium	*Conc* (10^{-3} *M*)	*Ea* (*kJ/mol*)	*ΔHa* (*kJ/mol*)	*ΔSa* (*kJ/mol.K*)
1.0 M HCl	***Blank***	21	18.46	−126.1
	MPQ	38.93	36.33	−87.36
	AAQ	27.24	24.64	−120.5

Moreover, the entropy values (ΔSa) observed during the rate-determining step reflect the level of disorder or randomness at the metal/solution interface [95]. The transition state of the rate-determining step generally exhibits a more ordered arrangement compared to the initial state, resulting in negative ΔSa values in the free acid solutions (blank). This indicates a decrease in disorder as the reagents move through the activated complex [34,95]. In the presence of inhibitors, however, the situation changes. The inhibitors adsorb onto the metal surface, coating it and influencing the hydrogen ion discharge [96]. This interference in the discharge process causes the system to transition from a more ordered to a more random state. Consequently, this change results in less negative ΔS values, suggesting an increase in disorder at the interface due to the presence of the inhibitors [96].

3.5. Contact angle

The outcomes from contact angle assessments (θ) conducted on steel specimens, both with and without the presence of the two inhibitors at their optimal concentrations, are outlined in Table 8.

Table 8 illustrates a notable rise in the contact angle (θ) for samples treated with MPQ and AAQ, as opposed to the control, indicating a decrease in surface hydrophilicity. This uptick in contact angle stems from the obstruction of the metal's active sites by absorbed inhibitor molecules, underscoring their inhibitory efficacy [97,98]. The order of inhibitor effectiveness, as determined by their contact angle (θ) at the optimal concentration, is as follows: AAQ > MPQ. These findings align well with the results obtained from both the electrochemical investigation and the adsorption isotherm study.

3.6. Scanning Electron Microscope with X-ray Dispersive Energy analysis

In order to deepen our understanding of the adsorption mechanisms

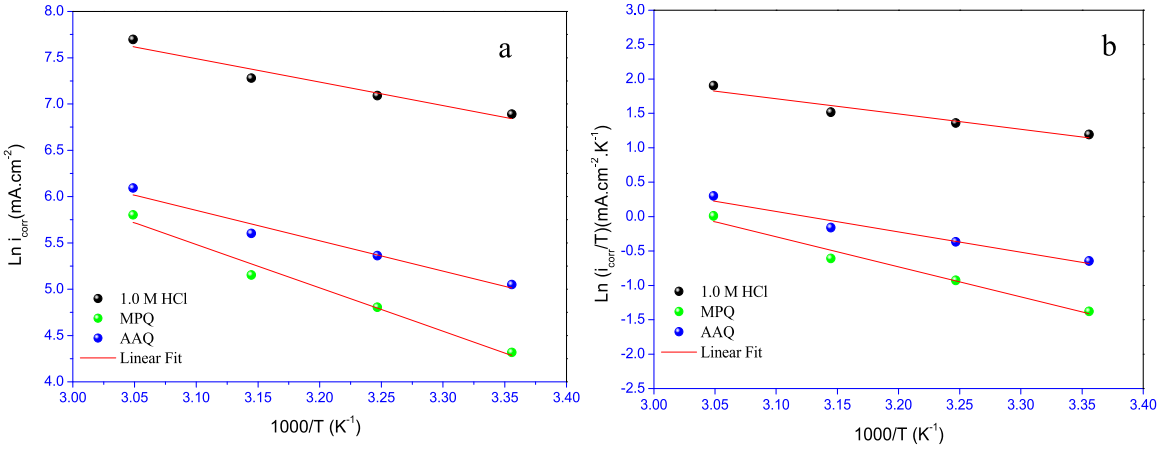

Fig. 9. Arrhenius Plots Comparing Mild Steel Corrosion in 1 M HCl with and without 10^{-3} M MPQ and AAQ.

Table 8
Measurements of contact angle for steel submerged in HCl (1.0 M) alone (blank) and with an optimal concentration of MPQ and AAQ for 24 h.

Blank	AAQ	MPQ
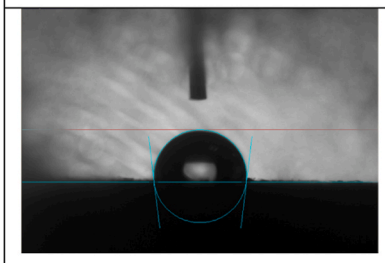	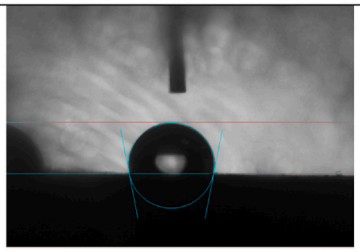	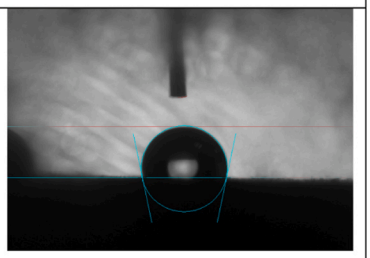
96°	101.5°	103°

involved in corrosion prevention, we conducted an analysis of the surface morphologies and EDX spectra of the mild steel substrate. The findings from this investigation are outlined in Table 9 and illustrated in Fig. 10.

Scanning electron microscope (SEM) images depict the steel coupon surface subsequent to immersion in a 1 M HCl medium, both in the absence and presence of our inhibitor. In the absence of the inhibitor, severe corrosion is evident, manifested by the roughened surface of the coupon. Conversely, images captured in the presence of our MPQ and AAQ inhibitors reveal an intact surface, with small particles of inhibitor film adhered to the steel surface. This observation suggests that the inhibitors shielded the coupon surface from corrosion induced by the aggressive environment. Energy dispersive X-ray (EDX) analysis was conducted to collect surface composition data of steel samples both before and after the introduction of MPQ and AAQ in a 1.0 M HCl solution. The resulting spectra from the EDX analysis are depicted in Fig. 10, while the atomic percentages are organized in Table 9.

However, immersing the steel in an HCl solution initiates autonomous degradation of the steel, evident from the emergence of an additional chloride peak in the EDX spectra, particularly notable in the blank case. Conversely, with the presence of MPQ and AAQ inhibitors, there is a slight decrease and disappearance of the oxygen and chlorine (Cl) peaks, respectively, as depicted in Fig. 10. Additionally, noteworthy is the appearance of an N peak in the MPQ case, indicating the adsorption of our inhibitors onto the surface of the metal under study.

3.7. Atomic Force Microscopy

AFM analysis allows for accurate measurement of the metal's surface roughness. In assessing the effectiveness of the compounds in preventing corrosion, steel substrates were immersion in corrosive environments for 24 hours, both before and after the addition of 10^{-3} M of MPQ and AAQ. The AFM-generated 3D images displaying surface morphology are shown in Table 10. The observable corrosion pits are likely indicative of steel degradation. However, the introduction of MPQ and AAQ resulted in a smoother, more uniform, and better-adhered surface [99,100]. The steel specimen, initially subjected to an acidic solution exhibited an average surface roughness of 50 nm, as depicted in Table 10. Upon introducing 10^{-3} M concentrations of MPQ and AAQ into the solution, notable reductions in roughness were observed, with values decreasing to 24 nm and 19 nm, respectively. This phenomenon underscores the efficacy of these compounds in mitigating surface roughness in acidic environments. Such reduction can be rationalized by the formation of a protective film facilitated by the interaction between the inhibitor molecules and the metal surface, as evidenced by prior research on corrosion inhibition mechanisms [101].

Table 9
Percentage mass of elements in substrate steel in 1.0 M HCl solution with and without MPQ and AAQ inhibitors at 298 K.

	C	O	N	Fe	Cl	Total
Blank	8.59	22.50	-	68.18	0.73	100
AAQ	7.90	21.80	-	70.3	-	100
MPQ	6.95	16.18	0.02	76.85	-	100

4. Theoretical methods

Theoretical computations are used to analyze and research a wide range of molecular characteristics. The Gaussian package program, which computes numerous quantum chemical parameters, is the most often utilized calculation technique to investigate the characteristics of molecules with these computations. The most significant of these computed values, the E_{HOMO} and E_{LUMO} parameters, let us discuss the activities of molecules. Two crucial factors that are utilized to explain the activities of molecules are the E_{HOMO} parameter, which indicates the ability of molecules to donate electrons [102], and the E_{LUMO} parameter, which displays the ability of molecules to absorb electrons [103]. All values are given in Tables 11 and 12 and molecule figures are given in Fig. 11. In theoretical calculations, calculations were made for the non-protonated and protonated states of MPQ(1) and AAQ(2) molecules in the gas phase and water phase.

In addition to this, the ΔE energy gap value is another measured parameter; a low numerical value of this parameter suggests that the molecule is more active [104]. Furthermore, electronegativity is the next metric, and its numerical value signifies that the lowest-lying molecule has a higher activity [103].

Various quantum chemical parameters, such as ΔE, EHOMO, ELUMO, chemical hardness, softness, electronegativity, and chemical potential, are often used to assess and evaluate the reactivity of molecules. These pertain to the ability of a chemical species to donate and accept electrons. Koopman's theorem [105] provides an alternative method for calculating the ionization energy and electron affinity of a chemical molecule, using boundary orbital energies.

In 1963, Pearson introduced the "chemical hardness" metric [106] as a means of measuring the ability of a chemical species to withstand deformation or polarization of its electron cloud. Theoretical and practical study consider the HSAB (Hard and Soft Acid-Base) [107] and PMH (Maximum Hardness Principle) [106] principles, which are based on the concept of chemical hardness. The classification of Lewis acids and bases into hard or soft categories is determined by the HSAB Principle. According to this principle, soft acids have a preference for coordinating with soft bases, whereas hard acids have a preference for coordinating with hard bases.

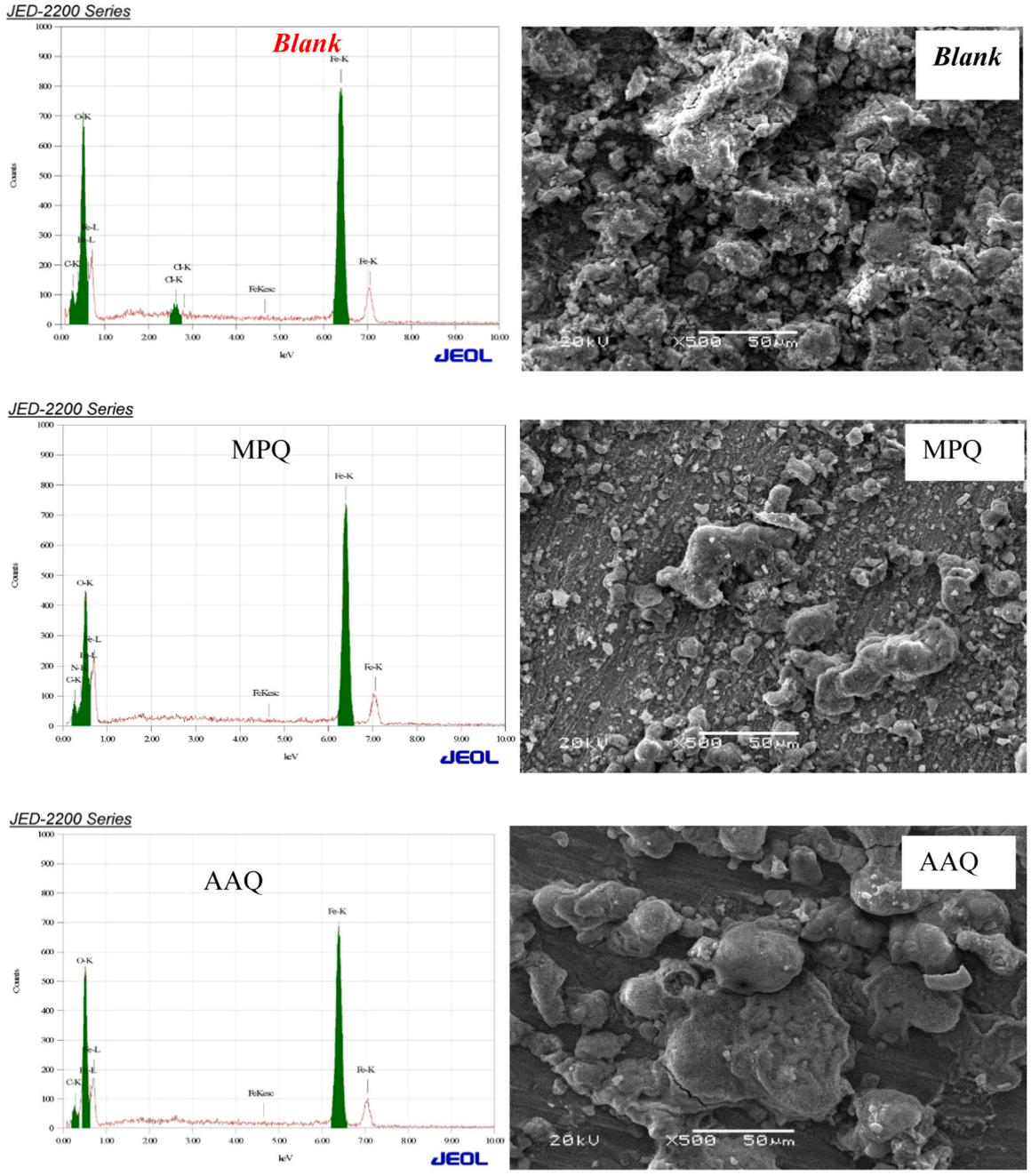

Fig. 10. SEM microscopy and EDX spectra obtained for mild steel surface pre and post 24-hour immersion in 1.0 M HCl solution, with and without MPQ and AAQ inhibitors, at 298 K.

Polarizable chemical species are denoted by the term "soft notion" in molecules, whereas non-polarizable chemical species are denoted by the term "hard notion". Molecules that are non-polarizable (hard) have challenges when it comes to transferring electrons to other molecules, whereas polarizable (soft) chemical species accomplish this easily [108]. The energy gap ΔE and chemical hardness are linked according to Koopman's theorem.

Hard molecules have a larger HOMO-LUMO gap, while soft molecules have a smaller HOMO-LUMO gap. Chemical hardness and softness are crucial attributes for assessing stability and reactivity. The measurement of a molecule's polarizability is determined by its softness (1/n), which is the inverse of chemical hardness. Soft molecules have higher reactivity compared to hard molecules due to their increased propensity to transfer electrons to an acceptor [109].

As a result of the gaussian calculations, many parameters of the molecules have been calculated, but not every parameter calculated has a formal representation. Fig. 11 shows the optimized structure of molecules, their HOMO, LUMO and distribution of Electrostatic potentials.

In theoretical calculations, calculations were made for both non-protonated and protonated states of MPQ(1) and AAQ(2) molecules in the gas phase and water phase. It was seen that many parameters were calculated as a result of the calculations. Among these parameters, the HOMO parameter of the molecules was found to be more positive in 8 of the calculations made at 9 levels in both the gas phase and the water phase in their non-protonated states. Naturally, it was understood that the AAQ molecule had higher activity than MPQ. On the other hand, when the numerical values of the LUMO parameter of the molecules were examined, the same order could not be seen. When the energy gap

Table 10
AFM analysis for mild steel surface in the absence and presence of MPQ and AAQ inhibitors.

Samples	3D AFM image	Average roughness
Blank	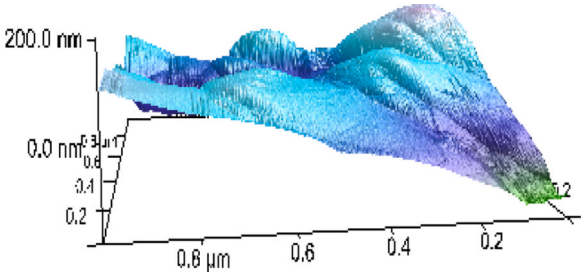	**50 nm**
MPQ	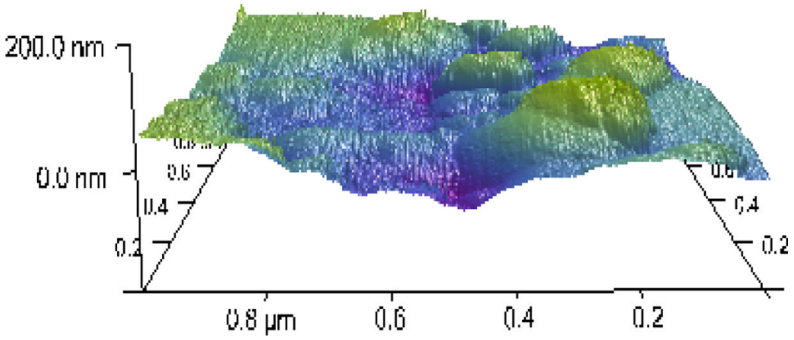	**24 nm**
AAQ	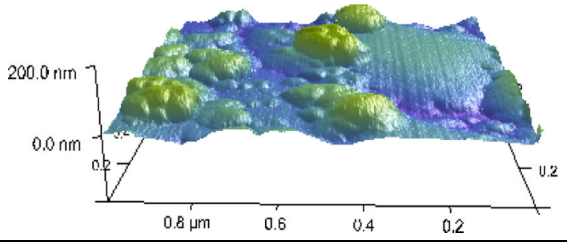	19. **m**

Table 11
The calculated quantum chemical parameters of molecules for non-protonated.

	E_{HOMO}	E_{LUMO}	I	A	ΔE	η	μ	χ	PA	ω	ε	dipol	Energy
B3LYP/6–31 g LEVEL													
1	−5.5661	−1.1388	5.5661	1.1388	4.4273	2.2137	0.4517	3.3525	−3.3525	2.5386	0.3939	3.2956	−20367.2302
2	−5.5495	−1.1247	5.5495	1.1247	4.4249	2.2124	0.4520	3.3371	−3.3371	2.5167	0.3973	2.7974	−20262.6297
B3LYP/6–31++g LEVEL													
1	−5.8589	−1.5086	5.8589	1.5086	4.3503	2.1752	0.4597	3.6838	−3.6838	3.1193	0.3206	3.6729	−20368.0526
2	−5.8276	−1.4800	5.8276	1.4800	4.3476	2.1738	0.4600	3.6538	−3.6538	3.0708	0.3256	3.5608	−20263.5857
B3LYP/6–31++g(d,p) LEVEL													
1	−5.7803	−1.4692	5.7803	1.4692	4.3111	2.1556	0.4639	3.6247	−3.6247	3.0476	0.3281	2.8841	−20374.4758
2	−5.7792	−1.4515	5.7792	1.4515	4.3277	2.1639	0.4621	3.6153	−3.6153	3.0202	0.3311	2.9583	−20270.1493
HF/6–31 g LEVEL													
1	−7.8032	2.5288	7.8032	−2.5288	10.3320	5.1660	0.1936	2.6372	−2.6372	0.6731	1.4856	3.9116	−20236.0604
2	−7.7744	2.5807	7.7744	−2.5807	10.3551	5.1776	0.1931	2.5968	−2.5968	0.6512	1.5356	3.5410	−20131.3947
HF/6–31++g LEVEL													
2	−7.9491	1.0022	7.9491	−1.0022	8.9513	4.4756	0.2234	3.4734	−3.4734	1.3478	0.7419	4.0319	−20236.5800
3	−7.9338	1.0036	7.9338	−1.0036	8.9374	4.4687	0.2238	3.4651	−3.4651	1.3435	0.7443	3.8292	−20132.0037
HF/6–31++g(d,p) LEVEL													
1	−7.8437	1.0398	7.8437	−1.0398	8.8835	4.4417	0.2251	3.4020	−3.4020	1.3028	0.7676	3.1008	−20245.8040
2	−7.8429	1.0373	7.8429	−1.0373	8.8802	4.4401	0.2252	3.4028	−3.4028	1.3039	0.7669	2.6441	−20141.2947
M062X/6–31 g LEVEL													
1	−6.8878	−0.2212	6.8878	0.2212	6.6666	3.3333	0.3000	3.5545	−3.5545	1.8952	0.5276	3.4143	−20358.4976
2	−6.8856	−0.2074	6.8856	0.2074	6.6783	3.3391	0.2995	3.5465	−3.5465	1.8834	0.5310	2.9400	−20254.0489
M062X/6–31++g LEVEL													
1	−7.1137	−0.5856	7.1137	0.5856	6.5281	3.2640	0.3064	3.8496	−3.8496	2.2701	0.4405	3.6784	−20359.1642
2	−7.1278	−0.5883	7.1278	0.5883	6.5395	3.2697	0.3058	3.8581	−3.8581	2.2761	0.4393	2.9819	−20254.8392
M062X/6–31++g(d,p) LEVEL													
1	−7.0364	−0.5587	7.0364	0.5587	6.4777	3.2389	0.3088	3.7975	−3.7975	2.2263	0.4492	2.8461	−20365.2154
2	−7.0146	−0.5214	7.0146	0.5214	6.4932	3.2466	0.3080	3.7680	−3.7680	2.1865	0.4573	3.0793	−20260.9447

Table 12
The calculated quantum chemical parameters of molecules for protonated.

	E_{HOMO}	E_{LUMO}	I	A	ΔE	η	μ	χ	PA	ω	ε	dipol	Energy
B3LYP/6–31 g LEVEL													
1	−3.0575	0.1165	3.0575	−0.1165	3.1740	1.5870	0.6301	1.4705	−1.4705	0.6813	1.4678	0.8469	−20382.8752
2	−1.3135	−0.9100	1.3135	0.9100	0.4035	0.2018	4.9560	1.1117	−1.1117	3.0627	0.3265	7.2890	−20275.6360
B3LYP/6–31++g LEVEL													
1	−3.3917	−0.4525	3.3917	0.4525	2.9391	1.4696	0.6805	1.9221	−1.9221	1.2570	0.7956	0.7269	−20383.7355
2	−2.5971	−1.6939	2.5971	1.6939	0.9032	0.4516	2.2145	2.1455	−2.1455	5.0968	0.1962	1.1193	−20277.3178
B3LYP/6–31++g(d,p) LEVEL													
1	−3.4085	−0.4351	3.4085	0.4351	2.9734	1.4867	0.6726	1.9218	−1.9218	1.2421	0.8051	1.0664	−20389.9617
2	−2.5780	−1.6569	2.5780	1.6569	0.9211	0.4606	2.1713	2.1175	−2.1175	4.8677	0.2054	1.6217	−20283.8054
HF/6–31 g LEVEL													
1	−5.9457	4.5411	5.9457	−4.5411	10.4868	5.2434	0.1907	0.7023	−0.7023	0.0470	21.259	0.7267	−20251.8273
2	−7.7744	2.5805	7.7744	−2.5805	10.3548	5.1774	0.1931	2.5969	−2.5969	0.6513	1.5354	3.5389	−20145.1354
HF/6–31++g LEVEL													
2	−7.9501	0.9241	7.9501	−0.9241	8.8742	4.4371	0.2254	3.5130	−3.5130	1.3907	0.7191	5.5236	−20250.6747
3	−3.5664	0.7671	3.5664	−0.7671	4.3334	2.1667	0.4615	1.3996	−1.3996	0.4521	2.2121	2.7985	−20144.9481
HF/6–31++g(d,p) LEVEL													
1	−7.8326	0.9636	7.8326	−0.9636	8.7961	4.3981	0.2274	3.4345	−3.4345	1.3410	0.7457	4.5808	−20259.8706
2	−3.5468	0.7872	3.5468	−0.7872	4.3340	2.1670	0.4615	1.3798	−1.3798	0.4393	2.2766	3.4077	−20154.2522
M062X/6–31 g LEVEL													
1	−4.1084	1.0768	4.1084	−1.0768	5.1852	2.5926	0.3857	1.5158	−1.5158	0.4431	2.2567	0.8867	−20374.0578
2	−1.9557	−0.2585	1.9557	0.2585	1.6972	0.8486	1.1784	1.1071	−1.1071	0.7222	1.3847	1.7708	−20266.7192
M062X/6–31++g LEVEL													
1	−4.3715	−0.1929	4.3715	0.1929	4.1786	2.0893	0.4786	2.2822	−2.2822	1.2465	0.8023	0.7912	−20374.7610
2	−3.2858	−0.7834	3.2858	0.7834	2.5024	1.2512	0.7992	2.0346	−2.0346	1.6543	0.6045	1.3281	−20268.2795
M062X/6–31++g(d,p) LEVEL													
1	−7.8326	0.9636	7.8326	−0.9636	8.7961	4.3981	0.2274	3.4345	−3.4345	1.3410	0.7457	4.5808	−20259.8706
2	−3.2493	−0.7622	3.2493	0.7622	2.4871	1.2436	0.8041	2.0058	−2.0058	1.6176	0.6182	1.8961	−20274.3481

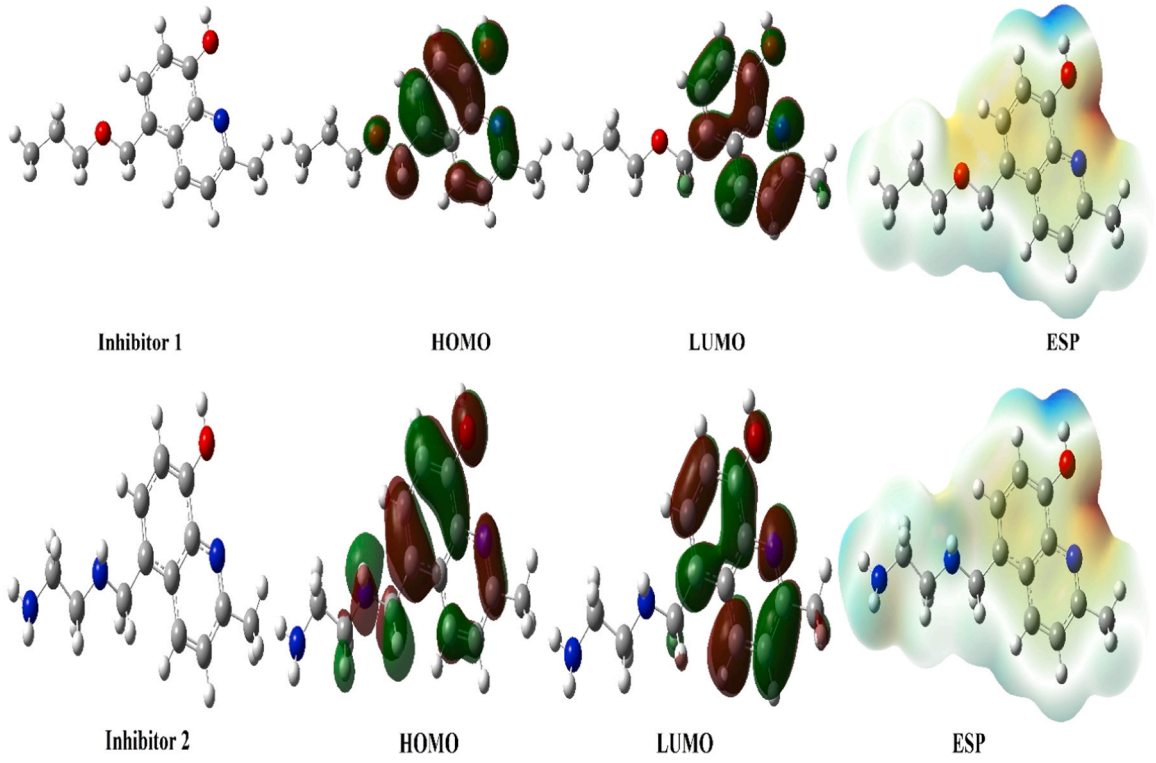

Fig. 11. Representations of optimize structure, HOMO, LUMO, and ESP of TM series.

values of the molecules were examined, it was seen that the activity of the AAQ molecule was higher in the non-protonated state at 3 levels in the gas phase and 9 levels in the water phase, and in the protonated state at 9 levels in the gas phase and 4 levels in the water phase. Finally, when the electronegativity values of the molecules were examined, it was seen that the AAQ molecule had high activity in both the gas phase and the water phase in non-protonated and protonated forms.

Electrostatic potential calculations provide important information about the stability, reactivity, and interactions of molecular systems [110]. For example, electrostatic potential calculations can be performed to determine the interaction domains of a molecule or to understand the interactions of a ligand with a protein. Additionally, such calculations can be used to analyze electrostatic interactions in molecular docking studies and drug design processes [111]. In these ESP

representations, it is known that the red regions are electron-rich regions and the blue regions are electron-poor regions.

To overcome the interactions between the investigated 5a and 5d species and metallic surfaces (Fe (110)). The side and top views of the stable adsorption configuration of 5a and 5d on the Fe (110) surface are shown in Fig. 12. Adsorption energies for 5a and 5d molecules on the Fe (110) surface, as seen in Fig. 12, indicate that the investigated organic species were positioned parallel to the metallic surface (Fe (110)), thereby enhancing their reactivity [112]. Additionally, the evaluated Eads value for 5a and 5d is −140.37 and −150.20 Kj mol^{-1} in Table 13. These negative Eads values reflect the high stability of the adsorption systems (Fe (110)/molecules). These results indicate the possibility of gradual substitution of water molecules from the Fe (110) surface and, consequently, the formation of a barrier film that can protect mild steel (M-S) from corrosion attack in the aqueous solution [113].

Observations indicate a gradual decrease in energy variation as the number of optimization steps increases. Initially, energy minimization is prominent owing to the instability of the molecular structure formula. However, in the later stages, total energy stabilizes as optimization progresses in Figs. 13a and 13b.

In Figs. 13a and 13b, we can observe the correlation between Forcite geometry optimization convergence and the quantity of optimization steps. This analysis employs the Conjugate Gradient optimization method while manipulating the molecular structure formula. From the graph, we can discern a progressive decline in both energy change and gradient value as optimization steps increase. This trend can be attributed to the gradual achievement of crystallization growth within the molecular structure formula under low-temperature crystallization conditions [114].

Energy distributions for 5a (a) and 5d (b) molecules on Fe (110) surface. such as total energy, average total energy, van der Waals energy, electrostatic energy, and intermolecular energy are presented in Fig. 14. The dominant form of interaction energy for the two adsorbents was van der Waals energy.

5. Conclusion

The study of the corrosion inhibition properties of MPQ and AAQ, both belonging to the quinoline family, has provided valuable information on their effectiveness in reducing corrosion in hydrochloric acid environments. Through meticulous experimentation and analysis, it has been demonstrated that:

- Both MPQ and AAQ operate through pure charge transfer kinetics.
- Both inhibitors were found to exhibit significant corrosion inhibition properties based on experimental analysis with an efficiency of 92.37 % for MPQ and 84.13 % for AAQ.
- Surface characterization techniques, including SEM-EDX, AFM, and contact angle measurements, demonstrated the formation of a protective barrier film that reduces the corrosion rate.
- Analysis of adsorption parameters and thermodynamic data revealed the protective mechanisms of MPQ and AAQ on mild steel surfaces. The inhibitors adhere to the steel surface by chemisorption, forming a protective film that serves as a barrier, effectively limiting the penetration of corrosive agents.
- Theoretical calculations, considering both protonated and unprotonated states, were utilized to provide accurate results for the acidic environment.
- In theoretical calculations, calculations were made for both non-protonated and protonated states of MPQ (1) and AAQ (2) molecules in the gas phase and water phase. It was seen that many parameters were calculated as a result of the calculations. When the numerical values of these parameters are examined, it is seen that the AAQ molecule has a high activity in the majority. One of the most important reasons for this is the nitrogen atoms found in the AAQ molecule and the lone electron pairs on these nitrogens. It is estimated from the HOMO values that it gives electron pairs to metal atoms using these electron pairs.
- Since the experimental studies were carried out in an acidic environment, the molecules were protonated to give more realistic

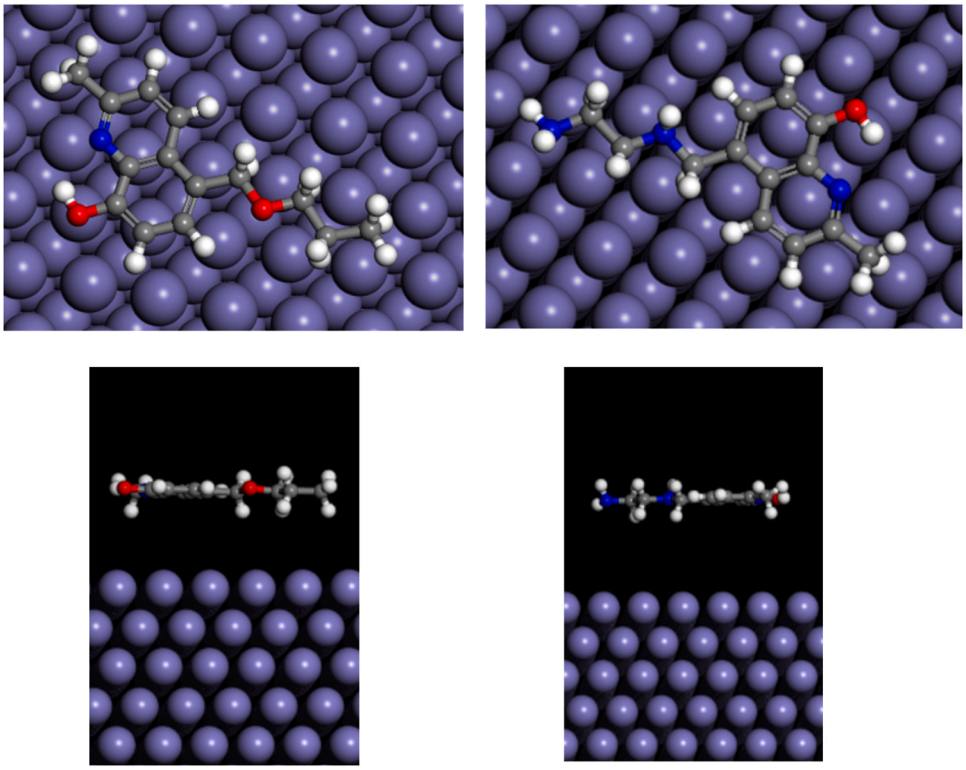

Fig. 12. Side and top views of the stable adsorption configuration of 5a and 5d on Fe (110) surface.

Table 13
The calculated quantum chemical parameters of molecules for non-protonated in water phase.

	E_{HOMO}	E_{LUMO}	I	A	ΔE	η	μ	χ	PA	ω	ε	dipol	Energy
B3LYP/6–31 g LEVEL													
1	−5.8279	−1.3883	5.8279	1.3883	4.4396	2.2198	0.4505	3.6081	−3.6081	2.9324	0.3410	4.601	−20367.6840
2	−5.7378	−1.3500	5.7378	1.3500	4.3879	2.1939	0.4558	3.5439	−3.5439	2.8623	0.3494	4.158	−20263.1297
B3LYP/6–31++g LEVEL													
1	−6.1215	−1.7356	6.1215	1.7356	4.3860	2.1930	0.4560	3.9285	−3.9285	3.5188	0.2842	5.408	−20368.5634
2	−6.0440	−1.7054	6.0440	1.7054	4.3386	2.1693	0.4610	3.8747	−3.8747	3.4603	0.2890	4.552	−20264.1649
B3LYP/6–31++g(d,p) LEVEL													
1	−6.0102	−1.6719	6.0102	1.6719	4.3383	2.1692	0.4610	3.8411	−3.8411	3.4008	0.2941	4.321	−20374.8703
2	−5.9773	−1.6455	5.9773	1.6455	4.3318	2.1659	0.4617	3.8114	−3.8114	3.3535	0.2982	3.643	−20270.6572
HF/6–31 g LEVEL													
1	−8.1199	2.2580	8.1199	−2.2580	10.3780	5.1890	0.1927	2.9310	−2.9310	0.8278	1.2081	5.457	−20236.6124
2	−8.0715	2.2983	8.0715	−2.2983	10.3698	5.1849	0.1929	2.8866	−2.8866	0.8035	1.2445	4.536	−20132.0065
HF/6–31++g LEVEL													
2	−8.2674	1.1549	8.2674	−1.1549	9.4223	4.7111	0.2123	3.5563	−3.5563	1.3423	0.7450	5.826	−20237.1591
3	−8.2236	1.1459	8.2236	−1.1459	9.3695	4.6847	0.2135	3.5389	−3.5389	1.3366	0.7481	4.698	−20132.6554
HF/6–31++g(d,p) LEVEL													
1	−8.1335	1.1551	8.1335	−1.1551	9.2887	4.6443	0.2153	3.4892	−3.4892	1.3107	0.7630	4.585	−20246.2509
2	−8.1028	1.1470	8.1028	−1.1470	9.2498	4.6249	0.2162	3.4779	−3.4779	1.3077	0.7647	3.659	−20141.8596
M062X/6–31 g LEVEL													
1	−7.1809	−0.4942	7.1809	0.4942	6.6867	3.3434	0.2991	3.8375	−3.8375	2.2024	0.4541	4.749	−20358.9879
2	−7.1303	−0.4593	7.1303	0.4593	6.6709	3.3355	0.2998	3.7948	−3.7948	2.1587	0.4632	4.251	−20254.5953
M062X/6–31++g LEVEL													
1	−7.4092	−0.8302	7.4092	0.8302	6.5789	3.2895	0.3040	4.1197	−4.1197	2.5797	0.3876	5.354	−20359.6994
2	−7.3656	−0.8041	7.3656	0.8041	6.5615	3.2808	0.3048	4.0849	−4.0849	2.5430	0.3932	4.534	−20255.4462
M062X/6–31++g(d,p) LEVEL													
1	−7.2998	−0.7802	7.2998	0.7802	6.5196	3.2598	0.3068	4.0400	−4.0400	2.5034	0.3995	4.235	−20365.6307
2	−3.3274	−0.2403	3.3274	0.2403	3.0872	1.5436	0.6478	1.7839	−1.7839	1.0308	0.9701	41.660	−20275.5286

Table 14
The calculated quantum chemical parameters of molecules for protonated in water phase.

	E_{HOMO}	E_{LUMO}	I	A	ΔE	η	μ	χ	PA	ω	ε	dipol	Energy
B3LYP/6–31 g LEVEL													
1	−6.6609	−2.8360	6.6609	2.8360	3.8249	1.9124	0.5229	4.7484	−4.7484	5.8950	0.1696	10.815	−20379.9707
2	−5.8344	−1.3984	5.8344	1.3984	4.4360	2.2180	0.4509	3.6164	−3.6164	2.9482	0.3392	33.634	−20275.3231
B3LYP/6–31++g LEVEL													
1	−6.8674	−3.0232	6.8674	3.0232	3.8442	1.9221	0.5203	4.9453	−4.9453	6.3618	0.1572	10.812	−20380.6165
2	−6.1272	−1.7475	6.1272	1.7475	4.3797	2.1899	0.4567	3.9374	−3.9374	3.5397	0.2825	34.367	−20276.1356
B3LYP/6–31++g(d,p) LEVEL													
1	−6.7765	−2.9789	6.7765	2.9789	3.7977	1.8988	0.5266	4.8777	−4.8777	6.2649	0.1596	11.079	−20386.8217
2	−6.0383	−1.6909	6.0383	1.6909	4.3473	2.1737	0.4601	3.8646	−3.8646	3.4355	0.2911	33.389	−20282.5402
HF/6–31 g LEVEL													
1	−9.2057	1.5233	9.2057	−1.5233	10.7290	5.3645	0.1864	3.8412	−3.8412	1.3752	0.7272	11.209	−20247.3064
2	−8.1363	2.2493	8.1363	−2.2493	10.3856	5.1928	0.1926	2.9435	−2.9435	0.8342	1.1987	33.938	−20144.1754
HF/6–31++g LEVEL													
2	−9.2775	1.0479	9.2775	−1.0479	10.3254	5.1627	0.1937	4.1148	−4.1148	1.6398	0.6098	11.275	−20247.7096
3	−8.2808	1.0264	8.2808	−1.0264	9.3072	4.6536	0.2149	3.6272	−3.6272	1.4136	0.7074	34.323	−20144.6837
HF/6–31++g(d,p) LEVEL													
1	−9.2125	1.0422	9.2125	−1.0422	10.2547	5.1273	0.1950	4.0851	−4.0851	1.6274	0.6145	12.080	−20256.6083
2	−8.1635	1.0291	8.1635	−1.0291	9.1926	4.5963	0.2176	3.5672	−3.5672	1.3842	0.7224	33.341	−20153.8986
M062X/6–31 g LEVEL													
1	−8.0340	−1.9649	8.0340	1.9649	6.0690	3.0345	0.3295	4.9995	−4.9995	4.1184	0.2428	10.969	−20371.1130
2	−7.1972	−0.5080	7.1972	0.5080	6.6892	3.3446	0.2990	3.8526	−3.8526	2.2189	0.4507	33.585	−20266.6841
M062X/6–31++g LEVEL													
1	−8.1847	−2.1350	8.1847	2.1350	6.0497	3.0248	0.3306	5.1599	−5.1599	4.4009	0.2272	10.999	−20371.6324
2	−7.4236	−0.8455	7.4236	0.8455	6.5781	3.2891	0.3040	4.1345	−4.1345	2.5987	0.3848	34.158	−20267.3419
M062X/6–31++g(d,p) LEVEL													
1	−9.2125	1.0422	9.2125	−1.0422	10.2547	5.1273	0.1950	4.0851	−4.0851	1.6274	0.6145	12.080	−20256.6083
2	−7.3333	−0.8038	7.3333	0.8038	6.5294	3.2647	0.3063	4.0685	−4.0685	2.5351	0.3945	33.111	−20273.3287

Table 15
Adsorption energies for 5a and 5d molecules on Fe (110) surface (Kj mol^{-1}).

System	Total energy	Adsorption energy	Rigid Adsorption energy	Deformation energy	dEad/dNi Molecule
5a	−79,03	−147,37	−139,34	−8,02	−147,37
5d	−58,67	−150,20	−137,63	−12,56	−150,20

results in theoretical calculations. Accordingly, the inhibitor activities of the molecules were compared. According to the numerical values of the obtained parameters, inhibitor MPQ was seen to have higher activity.

CRediT authorship contribution statement

Azzeddine Belkheiri: Writing – original draft, Writing – review & editing. **Khadija Dahmani:** Writing – original draft, Writing – review & editing. **Khaoula Mzioud:** Data curation, Formal analysis, Writing – original draft. **Abdelfettah Hmada:** Formal analysis, Funding

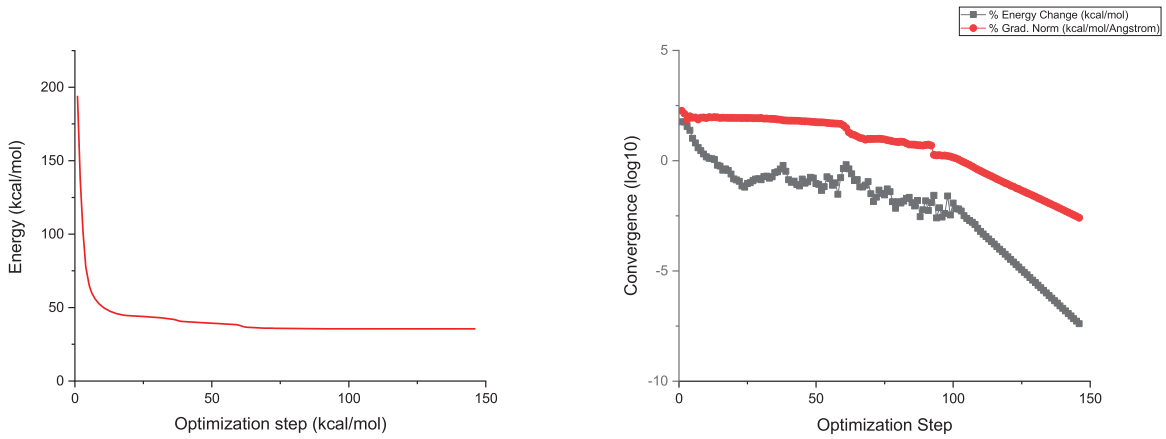

Fig. 13. a) Forcite geometry optimization of energy 5a molecule b) Forcite geometry optimization of convergence 5a molecule.

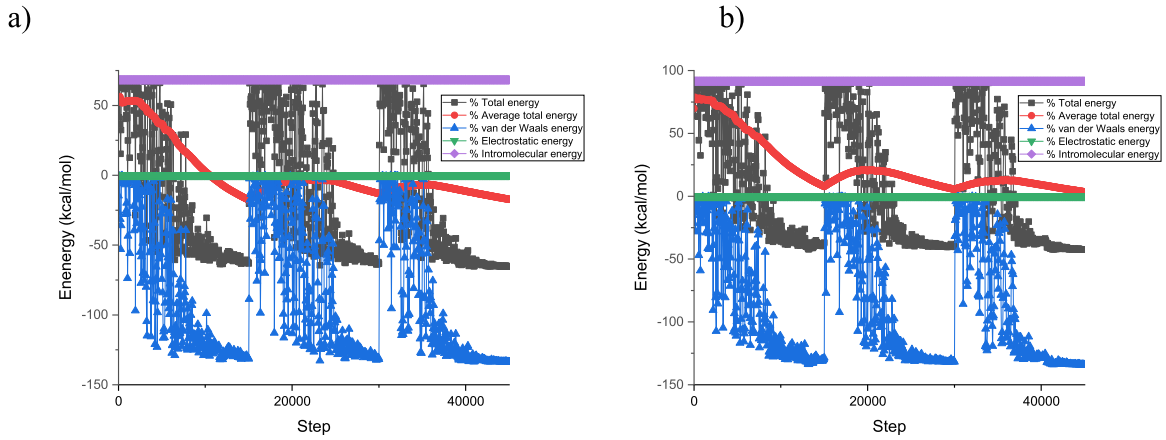

Fig. 14. Energy distributions for 5a (a) and 5d (b) molecules on Fe (110) surface.

acquisition, Methodology. **Mohamed Rbaa:** Methodology, Software. **Burak Tüzün:** Methodology, Software. **Şaban Erdoğan:** Methodology, Software. **Hamed A. El-Serehy:** Funding acquisition, Resources, Software, Validation. **Mohamed Ebn Touhami:** Supervision. **Mouhsine Galai:** Writing – review & editing, Validation, Supervision. **Basheer M. Al-Maswari:** Investigation, Software.

Declaration of Competing Interest

The authors declare that they have no known competing financial interests or personal relationships that could have appeared to influence the work reported in this paper.

Acknowledgements

The authors also extend their sincere appreciation to the Researchers Supporting Project Number (RSP2024R19), King Saud University, Riyadh, Saudi Arabia.

References

[1] G. Di Lorenzo, A. Formisano, G. Terracciano, R. Landolfo, Iron alloys and structural steels from XIX century until today: Evolution of mechanical properties and proposal of a rapid identification method, Constr. Build. Mater. 302 (2021) 124132, https://doi.org/10.1016/j.conbuildmat.2021.124132.

[2] D. Melzer, J. Džugan, M. Koukolikova, S. Rzepa, J. Vavřík, Structural integrity and mechanical properties of the Functionally Graded Material based on 316L/IN718 processed by DED technology, Mater. Sci. Eng. A 811 (2021) 141038, https://doi.org/10.1016/j.msea.2021.141038.

[3] S. Lyon, 1 - Overview of corrosion engineering, science and technology, in: D. Féron (Ed.), Nucl. Corros. Sci. Eng., Woodhead Publishing, 2012, pp. 3–30, https://doi.org/10.1533/9780857095343.1.3.

[4] N. Ferraa, M. Ouakki, H. El Harmouchi, M. Cherkaoui, M. Bennani Ziatni, Investigation of the inhibition behavior of an octacalcium phosphate as a green corrosion inhibitor against carbon steel in 3% NaCl medium, Inorg. Chem. Commun. 157 (2023), https://doi.org/10.1016/j.inoche.2023.111343.

[5] F. Mutahhar, G. Aithan, E.V. Iski, M.W. Keller, S. Shirazi, K.P. Roberts, 31 - Mechanistic modeling of erosion–corrosion for carbon steel, in: A.M. El-Sherik (Ed.), Trends Oil Gas Corros. Res. Technol., Woodhead Publishing, Boston, 2017, pp. 749–763, https://doi.org/10.1016/B978-0-08-101105-8.00031-0.

[6] K. Mzioud, A. Habsaoui, S. Rached, R. Lachhab, N. Dkhireche, M. Ouakki, M. Galai, E. Souad, M. Touhami, Synergistic Effect from Allium sativum Essential Oil and Diethylthiourea for Corrosion Inhibition of Carbon Steel in 0.5 M H2SO4 Medium, in: 2022: pp. 251–266. https://doi.org/10.1007/978-3-031-11397-0_23.

[7] N. Ferraa, M. Ouakki, M. Cherkaoui, M. Ziatni, Study of the Inhibitory Action of Apatitic Tricalcium Phosphate on Carbon Steel in Two Acidic Media (HCl 1.0 M and H2SO4 0.5 M), in: 2022: pp. 159–176. https://doi.org/10.1007/978-3-031-11397-0_14.

[8] C. Verma, M.A. Quraishi, E.E. Ebenso, Quinoline and its derivatives as corrosion inhibitors: A review, Surf. Interfaces 21 (2020) 100634, https://doi.org/10.1016/j.surfin.2020.100634.

[9] B.X. Vuong, T.L. Huynh, T.Q.N. Tran, S.V.P. Vattikuti, T.D. Manh, P. Nguyen-Tri, A.T. Nguyen, P. Van Hien, N. Nguyen Dang, Corrosion inhibition of carbon steel in hydrochloric acid solution by self-formation of a Malpighia glabra leaf extract-based organic film, Mater. Today Commun. 31 (2022) 103641, https://doi.org/10.1016/j.mtcomm.2022.103641.

[10] A.G. Bedir, M. Abd El-raouf, S. Abdel-Mawgoud, N.A. Negm, N.M. El Basiony, Corrosion Inhibition of Carbon Steel in Hydrochloric Acid Solution Using Ethoxylated Nonionic Surfactants Based on Schiff Base: Electrochemical and Computational Investigations, ACS Omega 6 (2021) 4300–4312, https://doi.org/10.1021/acsomega.0c05476.

[11] H. Mobtaker, M. Azadi, M. Rassouli, The corrosion inhibition of carbon steel in 1 M HCl solution by *Oestrus ovis* larvae extract as a new bio–inhibitor, Heliyon 8 (2022) e12297, https://doi.org/10.1016/j.heliyon.2022.e12297.

[12] M. Cui, Y. Yu, Y. Zheng, Effective Corrosion Inhibition of Carbon Steel in Hydrochloric Acid by Dopamine-Produced Carbon Dots, Polymers 13 (2021) 1923, https://doi.org/10.3390/polym13121923.
[13] N. Dkhireche, M. Galai, Y. El Kacimi, M. Rbaa, M. Ouakki, B. Lakhrissi, M. E. Touhami, New quinoline derivatives as sulfuric acid inhibitor's for mild steel, Anal. Bioanal. Electrochem 10 (2018) 111–135.
[14] M. Ouakki, H. Chahmout, S. Sibous, M. Galai, Z. Benzakri, S. Boukhris, A. Souizi, M. Cherkaoui, Novel pyrazole derivatives as inhibitors of stainless steel in 2.0M H2SO4 media: Electrochemical Study, Mediterr. J. Chem. 10 (2020) 239–252, https://doi.org/10.13171/mjc02003161235mo.
[15] Z. Aribou, M. Ouakki, N. Khemmou, S. Sibous, E. Ech-chihbi, Z. Benzekri, M. Galai, S. Boukhris, A.A. AlObaid, I. Warad, M.E. Touhami, Detailed experimental of indazole derivatives as corrosion inhibitor for brass in acidic environment: electrochemical/theoretical/surface studies, J. Appl. Electrochem. 54 (2024) 393–411, https://doi.org/10.1007/s10800-023-01960-6.
[16] K. Mzioud, A. Habsaoui, M. Ouakki, M. Galai, S. El Fartah, M. Ebn Touhami, Inhibition of copper corrosion by the essential oil of Allium sativum in 0.5M H2SO4 solutions, SN Appl. Sci. 2 (2020) 1611, https://doi.org/10.1007/s42452-020-03393-8.
[17] S. Rached, A. Habsaoui, K. Mzioud, R. Lachhab, S. Haida, N. Errahmany, M. Galai, M.E. Touhami, Valorization of the green corrosion inhibitor Marrubium vulgare L.: Electrochemical, thermodynamic, theoretical & surface studies, Chem. Data Collect. 48 (2023), https://doi.org/10.1016/j.cdc.2023.101099.
[18] L. Chen, D. Lu, Y. Zhang, Organic Compounds as Corrosion Inhibitors for Carbon Steel in HCl Solution: A Comprehensive Review, Materials 15 (2022) 2023, https://doi.org/10.3390/ma15062023.
[19] K. Dahmani, M. Galai, M. Ouakki, A. Elgendy, R. Ez-Zriouli, R. Lachhab, S. Briche, M. Cherkaoui, Corrosion inhibition of copper in sulfuric acid via environmentally friendly inhibitor (Myrtus communis): Combining experimental and theoretical methods, J. Mol. Liq. 347 (2022) 117982, https://doi.org/10.1016/j.molliq.2021.117982.
[20] B. Tan, Y. Liu, Z. Gong, X. Zhang, J. Chen, L. Guo, J. Xiong, J. Liu, R. Marzouki, W. Li, Pyracantha fortuneana alcohol extracts as biodegradable corrosion inhibitors for copper in H2SO4 media, J. Mol. Liq. 397 (2024) 124117, https://doi.org/10.1016/j.molliq.2024.124117.
[21] A.G. Sayed, A.M. Ashmawy, W.E. Elgammal, S.M. Hassan, M.A. Deyab, Synthesis, description, and application of novel corrosion inhibitors for CS AISI1095 in 1.0 M HCl based on benzoquinoline derivatives, Sci. Rep. 13 (2023) 13761, https://doi.org/10.1038/s41598-023-39714-1.
[22] H. Ren, Y. Liu, Z. Gong, B. Tan, H. Deng, J. Xiong, P. Shao, Q. Dai, J. Cao, R. Marzouki, Pumpkin Leaf Extract Crop Waste as a New Degradable and Environmentally Friendly Corrosion Inhibitor, Langmuir 40 (2024) 5738–5752, https://doi.org/10.1021/acs.langmuir.3c03399.
[23] M. Marinescu, Recent advances in the use of benzimidazoles as corrosion inhibitors, BMC Chem. 13 (2019) 136, https://doi.org/10.1186/s13065-019-0655-y.
[24] C. Verma, V.S. Saji, M.A. Quraishi, E.E. Ebenso, Pyrazole derivatives as environmental benign acid corrosion inhibitors for mild steel: Experimental and computational studies, J. Mol. Liq. 298 (2020) 111943, https://doi.org/10.1016/j.molliq.2019.111943.
[25] I. Singh, Inhibition of Steel Corrosion by Thiourea Derivatives, CORROSION 49 (1993) 473–478, https://doi.org/10.5006/1.3316074.
[26] J. Aljourani, K. Raeissi, M.A. Golozar, Benzimidazole and its derivatives as corrosion inhibitors for mild steel in 1M HCl solution, Corros. Sci. 51 (2009) 1836–1843, https://doi.org/10.1016/j.corsci.2009.05.011.
[27] Z. Huang, L. Liu, B. Lei, G. Meng, Z. Feng, H. Guo, B. Liao, P. Zhang, A New Imidazole Derivative for Corrosion Inhibition of Q235 Carbon Steel in an Acid Environment, Polymers 15 (2023) 2420, https://doi.org/10.3390/polym15112420.
[28] M.E. Faydy, R. Touir, M.E. Touhami, A. Zarrouk, C. Jama, B. Lakhrissi, L. O. Olasunkanmi, E.E. Ebenso, F. Bentiss, Corrosion inhibition performance of newly synthesized 5-alkoxymethyl-8-hydroxyquinoline derivatives for carbon steel in 1 M HCl solution: experimental, DFT and Monte Carlo simulation studies, Phys. Chem. Chem. Phys. 20 (2018) 20167–20187, https://doi.org/10.1039/C8CP03226B.
[29] L. Jiang, Y. Qiang, Z. Lei, J. Wang, Z. Qin, B. Xiang, Excellent corrosion inhibition performance of novel quinoline derivatives on mild steel in HCl media: Experimental and computational investigations, J. Mol. Liq. 255 (2018) 53–63, https://doi.org/10.1016/j.molliq.2018.01.133.
[30] Z.S. Erdoğan, S. Safi, D.Ö. Kaya, L. Işın, C. Guo, Kaya, A computational study on corrosion inhibition performances of novel quinoline derivatives against the corrosion of iron, J. Mol. Struct. 1134 (2017) 751–761, https://doi.org/10.1016/j.molstruc.2017.01.037.
[31] H. Fakhry, M. El Faydy, F. Benhiba, T. Laabaissi, M. Bouassiria, M. Allali, B. Lakhrissi, H. Oudda, A. Guenbour, I. Warad, A. Zarrouk, A newly synthesized quinoline derivative as corrosion inhibitor for mild steel in molar acid medium: Characterization (SEM/EDS), experimental and theoretical approach, Colloids Surf. Physicochem. Eng. Asp. 610 (2021) 125746, https://doi.org/10.1016/j.colsurfa.2020.125746.
[32] S. Kaya, B. Tüzün, C. Kaya, I.B. Obot, Determination of corrosion inhibition effects of amino acids: quantum chemical and molecular dynamic simulation study, J. Taiwan Inst. Chem. Eng. 58 (2016) 528–535.
[33] S. Kaya, L. Guo, C. Kaya, B. Tüzün, I.B. Obot, R. Touir, N. Islam, Quantum chemical and molecular dynamic simulation studies for the prediction of inhibition efficiencies of some piperidine derivatives on the corrosion of iron, J. Taiwan Inst. Chem. Eng. 65 (2016) 522–529.
[34] M. Galai, K. Dahmani, O. Kharbouch, M. Rbaa, N. Alzeqri, L. Guo, A.A. AlObaid, A. Hmada, N. Dkhireche, E. Ech-chihbi, M. Ouakki, M.E. Touhami, I. Warad, Surface analysis and interface properties of a newly synthesized quinoline-derivative corrosion inhibitor for mild steel in acid pickling bath: Mechanistic exploration through electrochemical, XPS, AFM, contact angle, SEM/EDS, and computational studies, J. Phys. Chem. Solids 184 (2024) 111681, https://doi.org/10.1016/j.jpcs.2023.111681.
[35] R. Dennington, T.A. Keith, J.M. Millam, GaussView, version 6.0. 16, Semichem Inc Shawnee Mission KS, 2016.
[36] Mj Frisch, G. Trucks, H. e al Schlegel, G.E. Scuseria, M.A. Robb, J.R. Cheeseman, J.A. Montgomery Jr, T. Vreven, K.N. Kudin, J.C. Burant, Gaussian 03, revision C. 02, (2004).
[37] A.D. Becke, Density-functional thermochemistry. I. The effect of the exchange-only gradient correction, J. Chem. Phys. 96 (1992) 2155–2160.
[38] D. Vautherin, D.M. Brink, Hartree-Fock Calculations with Skyrme's Interaction. I. Spherical Nuclei, Phys. Rev. C. 5 (1972) 626–647, https://doi.org/10.1103/PhysRevC.5.626.
[39] E.G. Hohenstein, S.T. Chill, C.D. Sherrill, Assessment of the Performance of the M05−2X and M06−2X Exchange-Correlation Functionals for Noncovalent Interactions in Biomolecules, J. Chem. Theory Comput. 4 (2008) 1996–2000, https://doi.org/10.1021/ct800308k.
[40] D. Majumdar, J.E. Philip, B. Gassoumi, S. Ayachi, B. Abdelaziz, B. Tüzün, S. Roy, Supramolecular clumps of μ2-1, 3-acetate bridges of Cd (II)-Salen complex: Synthesis, spectroscopic characterization, crystal structure, DFT quantization's, and antifungal photodynamic therapy., Heliyon (2024). https://www.cell.com/heliyon/fulltext/S2405-8440(24)05887-0 (accessed May 22, 2024).
[41] R. Haldhar, C.J. Raorane, V.K. Mishra, B. Tuzun, E. Berdimurodov, S.-C. Kim, Surface adsorption and corrosion resistance performance of modified chitosan: Gravimetric, electrochemical, and computational studies, Int. J. Biol. Macromol. 264 (2024) 130769.
[42] D. Douche, H. Elmsellem, L. Guo, B. Hafez, B. Tüzün, A. El Louzi, K. Bougrin, K. Karrouchi, B. Himmi, Anti-corrosion performance of 8-hydroxyquinoline derivatives for mild steel in acidic medium: Gravimetric, electrochemical, DFT and molecular dynamics simulation investigations, J. Mol. Liq. 308 (2020) 113042.
[43] E. Ech-Chihbi, A. Nahlé, R. Salim, F. Benhiba, A. Moussaif, F. El-Hajjaji, H. Oudda, A. Guenbour, M. Taleb, I. Warad, Computational, MD simulation, SEM/EDX and experimental studies for understanding adsorption of benzimidazole derivatives as corrosion inhibitors in 1.0 M HCl solution, J. Alloy. Compd. 844 (2020) 155842.
[44] R. Haldhar, D. Prasad, A. Saxena, A. Kaur, Corrosion resistance of mild steel in 0.5 M H2SO4 solution by plant extract of Alkana tinctoria: Experimental and theoretical studies, Eur. Phys. J. 133 (2018) 356, https://doi.org/10.1140/epjp/i2018-12165-0.
[45] R. Karthikaiselvi, S. Subhashini, Study of adsorption properties and inhibition of mild steel corrosion in hydrochloric acid media by water soluble composite poly (vinyl alcohol-*o*-methoxy aniline), J. Assoc. Arab Univ. Basic Appl. Sci. 16 (2014) 74–82, https://doi.org/10.1016/j.jaubas.2013.06.002.
[46] S. Rached, K. Mzioud, A. Habsaoui, M. Galai, K. Dahmani, M. Ouakki, S. El Fartah, N. Dkhireche, M. Ebn Touhami, Inhibition of Copper Corrosion in Sulfuric Acid by Mentha pulegium L., Port, Electrochim. Acta 42 (2024) 137–153, https://doi.org/10.4152/pea.2023420205.
[47] M. Ouakki, K. Dahmani, Z. Aribou, E. Ech-chihbi, M. Galai, N. AlZeqri, I. Warad, Z. Benzekri, L. Guo, A.A. AlObaid, O.H. Abd-Elkader, S. Boukhris, M. Cherkaoui, Adsorption of novel heterocyclic compounds of the purine derivatives as corrosion inhibitors over mild steel surface in acidic medium: Electrochemical, surface characterization and theoretical investigations, Inorg. Chem. Commun. 157 (2023) 111342, https://doi.org/10.1016/j.inoche.2023.111342.
[48] B. Tan, S. Zhang, Y. Qiang, W. Li, H. Liu, C. Xu, S. Chen, Insight into the corrosion inhibition of copper in sulfuric acid via two environmentally friendly food spices: Combining experimental and theoretical methods, J. Mol. Liq. 286 (2019) 110891, https://doi.org/10.1016/j.molliq.2019.110891.
[49] H. Jafari, E. Ameri, M. Hassan Vakili, A. Berisha, Effect of OH position on adsorption behavior of Schiff-base derivatives in corrosion inhibition of carbon steel in 1 M HCl, Electrochem. Commun. 159 (2024) 107653, https://doi.org/10.1016/j.elecom.2023.107653.
[50] H. Jia, H. Jia, Y. Lu, X. Li, C. Guo, C. Li, Z. Shen, P. Pei, H. Sun, K. Lv, P. Huang, Experimental and theoretical investigation of novel ammonium-derived dihydroxyl ionic liquid as corrosion inhibitor for mild steel in 1 M HCl: Effects of dihydroxyl and head groups, J. Mol. Liq. 402 (2024) 124777, https://doi.org/10.1016/j.molliq.2024.124777.
[51] S. John, Z.P. Mathew, C. Augustine, J.B. George, B. Joseph, M.K.S. Josh, Corrosion inhibition of mild steel in 1 M HCl using water soluble chitosan derivative of vanillin, Int. J. Biol. Macromol. 262 (2024) 130024, https://doi.org/10.1016/j.ijbiomac.2024.130024.
[52] A.H. Al-Moubaraki, H. Awaji, 1-X-4-[4\'-(-OCH 3)-Styryl] pyridinium iodides, potent inhibitors for stainless steel corrosion in 2 M HCl acid solutions, Int. J. Corros. Scale Inhib. 9 (2020) 460–501.
[53] G. Doumane, J. Bensalah, M. Ouakki, Z. Aribou, O. Boussalem, K. Mzioud, Z. S. Safi, A. Berisha, M. Bourhia, A.-R.Z. Gaafar, S. Ibenmoussa, G.F. Wondmie, A. Zarrouk, M.E. Touhami, A. Habsaoui, Alkaloid extract of seed Citrullus colocynthis as novel green inhibitor for mild steel corrosion in one molar HCl acid solution: DFT and MC/MD approaches, Sci. Rep. 14 (2024) 16857, https://doi.org/10.1038/s41598-024-67011-y.
[54] Z. El-kiri, A. Hmada, R. Sayed, K. Dakhsi, A. Larioui, F. Benhiba, R. Hsissou, N. Dkhireche, M. Galai, M. EbnTouhami, Correlation between experimental and

theoretical approaches in the performance of new epoxy resin as an effective corrosion inhibitor for mild steel in acid pickling bath, J. Mol. Struct. 1294 (2023) 136466, https://doi.org/10.1016/j.molstruc.2023.136466.
[55] K. Mzioud, A. Habsaoui, S. Rached, E. Ech-chihbi, M. Ouakki, R. Salghi, M. E. Touhami, Experimental Investigation and Theoretical Modeling of Copper Corrosion Inhibition by *Urginea maritima* Essential Oil, Mater. Today Sustain. (2024) 100906, https://doi.org/10.1016/j.mtsust.2024.100906.
[56] R.S. Al-Moghrabi, A.M. Abdel-Gaber, H.T. Rahal, A comparative study on the inhibitive effect of Crataegus oxyacantha and Prunus avium plant leaf extracts on the corrosion of mild steel in hydrochloric acid solution, Int. J. Ind. Chem. 9 (2018) 255–263, https://doi.org/10.1007/s40090-018-0154-3.
[57] M.A. Deyab, M.M. Abdeen, M. Hussien, I.E. El-Sayed, A. Galhoum, O.A.A. El-Shamy, M. Abd Elfattah, Novel Corrosion Inhibitor for Carbon Steel in Acidic Solutions Based on α-Aminophosphonate (Chemical, Electrochemical, and Quantum Studies), Molecules 28 (2023) 4962, https://doi.org/10.3390/molecules28134962.
[58] Y. Lou, W. Chang, T. Cui, H. Qian, L. Huang, L. Ma, X. Hao, D. Zhang, Microbiologically influenced corrosion inhibition of carbon steel via biomineralization induced by Shewanella putrefaciens, Npj Mater. Degrad. 5 (2021) 1–11, https://doi.org/10.1038/s41529-021-00206-0.
[59] M.H. Sliem, M. Afifi, A. Bahgat Radwan, E.M. Fayyad, M.F. Shibl, F.E.-T. Heakal, A.M. Abdullah, AEO7 Surfactant as an Eco-Friendly Corrosion Inhibitor for Carbon Steel in HCl solution, Sci. Rep. 9 (2019) 2319, https://doi.org/10.1038/s41598-018-37254-7.
[60] R.S. Al-Moghrabi, A.M. Abdel-Gaber, H.T. Rahal, Corrosion Inhibition of Mild Steel in Hydrochloric and Nitric Acid Solutions Using Willow Leaf Extract, Prot. Met. Phys. Chem. Surf. 55 (2019) 603–607, https://doi.org/10.1134/S2070205119030031.
[61] Y. Chen, Y. An, J. Ma, Z. Zhang, F. Qiao, X. Lei, F. Sun, C. Wang, S. Gao, Y. Zhao, J. Wang, X. Fu, H. Wang, Z. Yu, Corrosion protection properties of tetraphenylethylene-based inhibitors toward carbon steel in acidic medium, RSC Adv. 13 (2023) 8317–8326, https://doi.org/10.1039/D2RA08062A.
[62] A. Singh, E.E. Ebenso, M.A. Quraishi, Corrosion Inhibition of Carbon Steel in HCl Solution by Some Plant Extracts, Int. J. Corros. 2012 (2012) e897430, https://doi.org/10.1155/2012/897430.
[63] G. Mayakrishnan, K. Devarayan, V. Ramani, N. Sulochana, An investigation of mild carbon steel corrosion inhibition in hydrochloric acid medium by environment friendly green inhibitors, J. Coat. Technol. Res. (2011).
[64] B. Tan, A. Fu, L. Guo, Y. Ran, J. Xiong, R. Marzouki, W. Li, Insight into anti-corrosion mechanism of Dalbergia odorifera leaves extract as a biodegradable inhibitor for X70 steel in sulfuric acid medium, Ind. Crops Prod. 194 (2023) 116106, https://doi.org/10.1016/j.indcrop.2022.116106.
[65] R. De Motte, E. Basilico, R. Mingant, J. Kittel, F. Ropital, P. Combrade, S. Necib, V. Deydier, D. Crusset, S. Marcelin, A study by electrochemical impedance spectroscopy and surface analysis of corrosion product layers formed during CO2 corrosion of low alloy steel, Corros. Sci. 172 (2020) 108666, https://doi.org/10.1016/j.corsci.2020.108666.
[66] B. Tan, Z. Gong, W. He, J. Xiong, L. Guo, R. Marzouki, Insight into the anti-corrosion mechanism of crop waste *Arachis hypogaea L.* leaf extract for copper in sulfuric acid medium, Sustain. Chem. Pharm. 38 (2024) 101449, https://doi.org/10.1016/j.scp.2024.101449.
[67] M.A. Bedair, A.M. Abuelela, M. Alshareef, M. Owda, E.M. Eliwa, Ethyl ester/acyl hydrazide-based aromatic sulfonamides: facile synthesis, structural characterization, electrochemical measurements and theoretical studies as effective corrosion inhibitors for mild steel in 1.0 M HCl, RSC Adv. 13 (2022) 186–211, https://doi.org/10.1039/D2RA05939H.
[68] A. Popova, M. Christov, A. Vasilev, Mono- and dicationic benzothiazolic quaternary ammonium bromides as mild steel corrosion inhibitors. Part III: Influence of the temperature on the inhibition process, Corros. Sci. 94 (2015) 70–78, https://doi.org/10.1016/j.corsci.2015.01.039.
[69] A.M. Abdel-Gaber, H.T. Rahal, F.T. Beqai, Eucalyptus leaf extract as a eco-friendly corrosion inhibitor for mild steel in sulfuric and phosphoric acid solutions, Int. J. Ind. Chem. 11 (2020) 123–132, https://doi.org/10.1007/s40090-020-00207-z.
[70] M.P. Chakravarthy, K.N. Mohana, Adsorption and Corrosion Inhibition Characteristics of Some Nicotinamide Derivatives on Mild Steel in Hydrochloric Acid Solution, Int. Sch. Res. Not. 2014 (2014) e687276, https://doi.org/10.1155/2014/687276.
[71] D. Özkır, K. Kayakırılmaz, E. Bayol, A.A. Gürten, F. Kandemirli, The inhibition effect of Azure A on mild steel in 1 M HCl. A complete study: Adsorption, temperature, duration and quantum chemical aspects, Corros. Sci. 56 (2012) 143–152, https://doi.org/10.1016/j.corsci.2011.11.010.
[72] H.T. Rahal, A.M. Abdel-Gaber, R. Awad, B.A. Abdel-Naby, Influence of nitrogen immersion and NiO nanoparticles on the electrochemical behavior of (Bi, Pb)-2223 superconductor in sodium sulfate solution, Anti-Corros, Methods Mater. 65 (2018) 430–435.
[73] H.T. Rahal, A.M. Abdel-Gaber, R. Awad, Influence of SnO2 nanoparticles incorporation on the Electrochemical Behaviour of a Superconductor in Sodium Sulphate Solutions, Int. J. Electrochem. Sci. 12 (2017) 10115–10128.
[74] S. El-Housseiny, A.M. Abdel-Gaber, H.T. Rahal, F.T. Beqai, Eco-friendly corrosion inhibitor for mild steel in acidic media, Int. J. Corros. Scale Inhib. (2022) 11, https://ijcsi.pro/papers/eco-friendly-corrosion-inhibitor-for-mild-steel-in-acidic-media/ (accessed August 16, 2024).
[75] Q. Li, Y. Zhang, Y. Cheng, X. Zuo, Y. Wang, X. Yuan, H. Huang, Effect of Temperature on the Corrosion Behavior and Corrosion Resistance of Copper–Aluminum Laminated Composite Plate, Materials 15 (2022) 1621, https://doi.org/10.3390/ma15041621.
[76] Y. Cai, Y. Zhao, X. Ma, K. Zhou, Y. Chen, Influence of environmental factors on atmospheric corrosion in dynamic environment, Corros. Sci. 137 (2018) 163–175, https://doi.org/10.1016/j.corsci.2018.03.042.
[77] A. Dahmani, Et-Touhami, S.S. Al-Deyab, B. Hammouti, A. Bouyanzer, Int J. Electrochem Sci. 5 (2010) 1060.
[78] Z. Aribou, M. Ouakki, N. Khemmou, S. Sibous, E. Ech-chihbi, O. Kharbouch, M. Galai, A. Souizi, S. Boukhris, M.E. Touhami, A.A. AlObaid, I. Warad, Exploring the adsorption and corrosion inhibition properties of indazole as a corrosion inhibitor for brass alloy in HCl medium: A theoretical and experimental study, Mater. Today Commun. 37 (2023), https://doi.org/10.1016/j.mtcomm.2023.107061.
[79] I.A. Adejoro, F.K. Ojo, S.K. Obafemi, Corrosion inhibition potentials of ampicillin for mild steel in hydrochloric acid solution, J. Taibah Univ. Sci. 9 (2015) 196–202, https://doi.org/10.1016/j.jtusci.2014.10.002.
[80] A.F.S. Abdul Rahiman, S. Sethumanickam, Corrosion inhibition, adsorption and thermodynamic properties of poly(vinyl alcohol-cysteine) in molar HCl, Arab. J. Chem. 10 (2017) S3358–S3366, https://doi.org/10.1016/j.arabjc.2014.01.016.
[81] E. Kuş, F. Mansfeld, An evaluation of the electrochemical frequency modulation (EFM) technique, Corros. Sci. - Corros. Sci. 48 (2006) 965–979, https://doi.org/10.1016/j.corsci.2005.02.023.
[82] E. Randviir, C. Banks, Electrochemical impedance spectroscopy: An overview of bioanalytical applications, Anal. Methods 5 (2013) 1098–1115, https://doi.org/10.1039/c3ay26476a.
[83] I.B. Obot, I.B. Onyeachu, Electrochemical frequency modulation (EFM) technique: Theory and recent practical applications in corrosion research, J. Mol. Liq. 249 (2018) 83–96, https://doi.org/10.1016/j.molliq.2017.11.006.
[84] K. Shalabi, A. Fouda, A. Alsallai, Thymus vulgarise Extract as Nontoxic Corrosion Inhibitor for Copper and α-Brass in 1 M HNO3 Solutions, Int. J. Electrochem. Sci. 9 (2014) 5126.
[85] A.A. Al-Amiery, A.B. Mohamad, A.A.H. Kadhum, L.M. Shaker, W.N.R.W. Isahak, M.S. Takriff, Experimental and theoretical study on the corrosion inhibition of mild steel by nonanedioic acid derivative in hydrochloric acid solution, Sci. Rep. 12 (2022) 4705, https://doi.org/10.1038/s41598-022-08146-8.
[86] A. Singh, V. Singh, M. Quraishi, Inhibition of Mild Steel Corrosion in HCl Solution Using Pipali (Piper longum) Fruit Extract, Arab. J. Sci. Eng. 38 (2012) 85–97, https://doi.org/10.1007/s13369-012-0409-9.
[87] M. Salavati-Niasari, sayed mehdi Ghoreishi, N. Soltani, M. Hamadanian, A. Gandomi, Electrochemical and theoretical investigation on the corrosion inhibition of mild steel by thiosalicylaldehyde derivatives in hydrochloric acid solution, Corros. Sci. - Corros. Sci. 50 (2008) 2172–2181, https://doi.org/10.1016/j.corsci.2008.06.020.
[88] H. Bahron, A.A. Ghani, E.H. Anouar, Z. Embong, A.I. Alharthi, M.K. Harun, Y. Alias, Adsorption, electrochemistry, DFT and inhibitive effect of imines derived from tribulin on corrosion of mild steel in 1 M HCl, J. Mol. Struct. 1235 (2021) 130206, https://doi.org/10.1016/j.molstruc.2021.130206.
[89] A. Singh, K.R. Ansari, M.A. Quraishi, Chondroitin sulfate as a green corrosion inhibitor for zinc in 26% ammonium chloride solution: Electrochemical and surface morphological analysis, Colloids Surf. Physicochem. Eng. Asp. 607 (2020) 125465, https://doi.org/10.1016/j.colsurfa.2020.125465.
[90] H. Chahmout, M. Ouakki, S. Sibous, M. Galai, N. Arrousse, E. Ech-chihbi, Z. Benzekri, S. Boukhris, A. Souizi, M. Cherkaoui, New pyrazole compounds as a corrosion inhibitor of stainless steel in 2.0 M H2SO4 medium: Electrochemical and theoretical insights, Inorg. Chem. Commun. 147 (2023) 110150.
[91] H. Lgaz, S. Masroor, M. Chafiq, M. Damej, A. Brahmia, R. Salghi, M. Benmessaoud, I.H. Ali, M.M. Alghamdi, A. Chaouiki, I.-M. Chung, Evaluation of 2-Mercaptobenzimidazole Derivatives as Corrosion Inhibitors for Mild Steel in Hydrochloric Acid, Metals 10 (2020) 357, https://doi.org/10.3390/met10030357.
[92] W. Gong, B. Xu, X. Yin, Y. Liu, Y. Chen, W. Yang, Halogen-substituted thiazole derivatives as corrosion inhibitors for mild steel in 0.5 M sulfuric acid at high temperature, J. Taiwan Inst. Chem. Eng. 97 (2019) 466–479.
[93] N. Ferraa, M. Ouakki, M. Cherkaoui, M. Bennani-Ziatni, Synthesis, Characterization and Evaluation of Apatitic Tricalcium Phosphate as a Corrosion Inhibitor for Carbon Steel in 3 wt% NaCl, J. Bio- Tribo-Corros. 8 (2022), https://doi.org/10.1007/s40735-021-00622-4.
[94] O.A. Akinbulumo, O.J. Odejobi, E.L. Odekanle, Thermodynamics and adsorption study of the corrosion inhibition of mild steel by *Euphorbia heterophylla L.* extract in 1.5 M HCl, Results Mater. 5 (2020) 100074, https://doi.org/10.1016/j.rinma.2020.100074.
[95] A. Ech-chebab, M. Missioui, L. Guo, O. El Khouja, R. Lachhab, O. Kharbouch, M. Galai, M. Ouakki, A. Ejbouh, K. Dahmani, N. Dkhireche, M. Ebn Touhami, Evaluation of quinoxaline-2(1H)-one, derivatives as corrosion inhibitors for mild steel in 1.0 M acidic media: Electrochemistry, quantum calculations, dynamic simulations, and surface analysis, Chem. Phys. Lett. 809 (2022) 140156, https://doi.org/10.1016/j.cplett.2022.140156.
[96] A.H. Al-Moubaraki, A. Chaouiki, J.M. Alahmari, W.A. Al-hammadi, E.A. Noor, A. A. Al-Ghamdi, Y.G. Ko, Development of Natural Plant Extracts as Sustainable Inhibitors for Efficient Protection of Mild Steel: Experimental and First-Principles Multi-Level Computational Methods, Materials 15 (2022) 8688, https://doi.org/10.3390/ma15238688.
[97] J. Wang, J. Jing, L. Feng, H. Zhu, Z. Hu, X. Ma, Study on corrosion inhibition behavior and adsorption mechanism of novel synthetic surfactants for carbon steel in 1 M HCl solution, Sustain. Chem. Pharm. 23 (2021) 100500, https://doi.org/10.1016/j.scp.2021.100500.
[98] Y. Qiang, S. Fu, S. Zhang, S. Chen, X. Zou, Designing and fabricating of single and double alkyl-chain indazole derivatives self-assembled monolayer for corrosion

inhibition of copper, Corros. Sci. 140 (2018) 111–121, https://doi.org/10.1016/j.corsci.2018.06.012.
[99] J. Lazrak, E.H. El Assiri, N. Arrousse, F. El-Hajjaji, M. Taleb, Z. Rais, A. Farah, A. Ramzi, B. Hammouti, Origanum compactum essential oil as a green inhibitor for mild steel in 1 M hydrochloric acid solution: Experimental and Monte Carlo simulation studies, Mater. Today Proc. 45 (2021) 7486–7493, https://doi.org/10.1016/j.matpr.2021.02.233.
[100] S. Zeinali Nikoo, A. Shockravi, H. Mokarami Ghartavol, A.Z. Halimehjani, M. Ostadrahimi, S.M. Mirhosseini, H. Behzadi, M. Ghorbani, A study of glycine-based dithiocarbamates as effective corrosion inhibitors for cold rolled carbon steel in HCl solutions, Surf. Interfaces 21 (2020) 100751, https://doi.org/10.1016/j.surfin.2020.100751.
[101] M. Tang, J. Li, Z. Li, L. Fu, B. Zeng, J. Lv, Mannich Base as Corrosion Inhibitors for N80 Steel in a CO2 Saturated Solution Containing 3 wt% NaCl, Materials 12 (2019) 449, https://doi.org/10.3390/ma12030449.
[102] K. Zerrouki, R. Bouchene, B. Tüzün, P. Retailleau, Novel supramolecular co-crystal of 8-hydroxyquinoline with acetone-(2, 4-dinitrophenyl) hydrazone: One pot synthesis, structural characterization, Hirshfeld surface and energy framework analysis, computational investigation and molecular docking study, J. Mol. Struct. 1300 (2024) 137290.
[103] I.O. Arukalam, I.N. Uzochukwu, B. Tüzün, O. Dagdag, E.E. Oguzie, Influence of ZnO Nanoparticle Size on Barrier Performance and Corrosion Protection of Poly (dimethylsiloxane)-Coated Q235 Steel in Chloride Environment: Bode and Computational Simulation Investigations, Chem. Afr. 7 (2024) 853–863, https://doi.org/10.1007/s42250-023-00791-4.
[104] V. Eyupoglu, A. Aksu, H.F. Çetinkaya, H.İ. Çetintaş, S. Çetinkaya, B. Tüzün, Biosorption of dye crystal violet on Tragopogon sp. leaf powder: Equilibrium, kinetics, thermodynamics, and DFT calculations, J. Mol. Liq. (2024) 124226.
[105] T. Schrader, J. Khanifaev, E. Perlt, Koopmans' theorem for acidic protons, Chem. Commun. 59 (2023) 13839–13842.
[106] R.G. Pearson, Hard and Soft Acids and Bases, J. Am. Chem. Soc. 85 (1963) 3533–3539, https://doi.org/10.1021/ja00905a001.
[107] R.G. Parr, P.K. Chattaraj, Principle of maximum hardness, J. Am. Chem. Soc. 113 (1991) 1854–1855, https://doi.org/10.1021/ja00005a072.
[108] P.W. Ayers, An elementary derivation of the hard/soft-acid/base principle, J. Chem. Phys. 122 (2005) https://pubs.aip.org/aip/jcp/article/122/14/141102/914285 (accessed August 16, 2024).
[109] J.C. Phillips, Generalized Koopmans' Theorem, Phys. Rev. 123 (1961) 420–424, https://doi.org/10.1103/PhysRev.123.420.
[110] D. Majumdar, S. Roy, J.E. Philip, B. Tüzün, S. Hazra, In-situ Salen-type ligand formation-driven of a heterometallic Cu (II)-Hg (II) complex: Synthetic update, crystallographic features, DFT calculations, and unveil antimicrobial profiles, Inorg. Chem. Commun. 160 (2024) 111933.
[111] I.O. Arukalam, I.N. Uzochukwu, V.O. Izionworu, B. Tüzün, O. Dagdag, Corrosion protection of Q235 steel in Pseudomonas aeruginosa-laden seawater environment using high barrier PDMS nanocomposite coating, Saf. Extrem. Environ. 5 (2023) 281–291, https://doi.org/10.1007/s42797-023-00087-3.
[112] Y. Fernine, N. Arrousse, R. Haldhar, C.J. Raorane, E. Ech-Chihbi, S.-C. Kim, F. El Hajjaji, A. Alami, M.E. Touhami, M. Taleb, Novel thiophene derivatives as eco-friendly corrosion inhibitors for mild steel in 1 M HCl solution: Characterization, electrochemical and computational (DFT and MC simulations) methods, J. Environ. Chem. Eng. 10 (2022) 108891.
[113] N. Arrousse, R. Salim, Y. Kaddouri, D. Zahri, F. El Hajjaji, R. Touzani, M. Taleb, S. Jodeh, The inhibition behavior of two pyrimidine-pyrazole derivatives against corrosion in hydrochloric solution: Experimental, surface analysis and in silico approach studies, Arab. J. Chem. 13 (2020) 5949–5965.
[114] T. Karmakar, P.M. Piaggi, M. Parrinello, Molecular Dynamics Simulations of Crystal Nucleation from Solution at Constant Chemical Potential, J. Chem. Theory Comput. 15 (2019) 6923–6930, https://doi.org/10.1021/acs.jctc.9b00795.